Table 2. Value of non-invasive parameters for the diagnosis of marked fibrosis, advanced fibrosis and cirrhosis: comparison of AUC among time interval, APRI, and FIB4

	Marked fibrosis (≥F2)	Advanced fibrosis (≥F3)	Cirrhosis
Time interval	0.94 (0.89–0.97)	0.96 (0.93–0.98)	0.98 (0.95–0.99)
APRI	0.86 (0.79–0.91)	0.85 (0.78–0.90)	0.80 (0.71–0.86)
FIB4	0.85 (0.79–0.91)	0.89 (0.82–0.94)	0.90 (0.82–0.95)

AUC, areas under the receiver operating characteristic curves; marked fibrosis, ≥F2; advanced fibrosis, ≥F3; time interval, time interval from the onset of contrast enhancement in the right portal vein to the time of the maximum intensity ratio between right portal vein and liver parenchyma.

decreased and the time interval from the onset of contrast enhancement in the right portal vein to the time of the maximum intensity ratio was prolonged according to the progression of hepatic fibrosis, and particularly the latter, being superior to both APRI and FIB4, had the closest relationship with the degree of hepatic fibrosis. Because the flow velocity in the right portal vein in our study tended to decrease according to the progression of hepatic fibrosis, as also reported previously (10), the rate of filling the right portal vein with microbubbles may be lower. Meanwhile, an arterialization related to hepatic fibrosis may compensate the rapid parenchymal enhancement with high blood flow (24). These factors may explain the decrease of the maximum intensity ratio between the right portal vein and liver parenchyma and prolongation of time interval from the onset of contrast enhancement in the right portal vein to the time of the maximum intensity ratio, according to the progression of fibrosis. However, despite the maximum intensity ratio between the right portal vein and liver parenchyma, time interval from the onset of contrast enhancement in the right portal vein to the time of the maximum intensity ratio did show a close relationship with the progression of fibrosis. The former parameter represents only the peak gradient of microbubble distribution between the portal vein and liver parenchyma, while the latter parameter is coupled with time. Although the precise mechanism remains unclear, time-related haemodynamics, linked to the microbubble distribution from the upstream vessel to the periphery, might have the advantage of indicating the degree of hepatic fibrosis. In fact, it is suggested that several pathophysiological conditions, such as the presence of intrahepatic shunt and/or hyperdynamic circulatory state (11), affected the parameters measured in this study. However, we believe that time interval from the onset of contrast enhancement in the right portal vein to the time of the maximum intensity ratio may represent an indirect parameter for assessing the degree of hepatic fibrosis in a comprehensive manner. Contrast-enhanced US with Sonazoid™ may have the possibility to reduce the biopsy procedure to examine the severity of hepatic fibrosis.

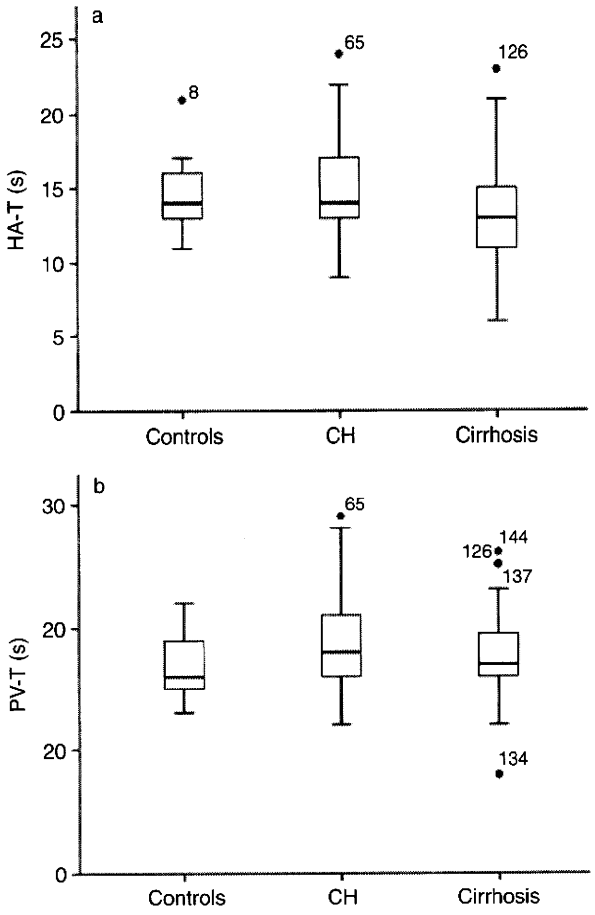

Fig. 4. Onset time of contrast enhancement in the right hepatic artery and the right portal vein. (a) Onset time of contrast enhancement in the right hepatic artery (s): there were no significant differences of the onset time of contrast enhancement in the right hepatic artery among the three groups ($P=0.0929$). (b) Onset time of contrast enhancement in the right portal vein (s): there were no significant differences of the onset time of contrast enhancement in the right portal vein among three groups ($P=0.1564$). Data are expressed by box-and-whisker plots. The top and bottom of the boxes indicate upper and lower quartiles, respectively, and the horizontal line in the bar represents the median value. The two horizontal lines outside the box (whisker) indicate the smallest and largest nonoutlier observations.

We also examined the two parameters, onset time of contrast enhancement in the right hepatic artery and right portal vein, which did not show significant correlation with the degree of hepatic fibrosis. The previous study reported similar results, in spite of the usage of different contrast agents (21). As these parameters may be affected by general conditions of systemic circulation as well as specific conditions caused by portal hypertension such as intrapulmonary shunt, hyperdynamic state, splenomegaly and development of extrahepatic collateral vessels, they may not be ideal factors to assess the degree of hepatic fibrosis.

Liver International (2010)

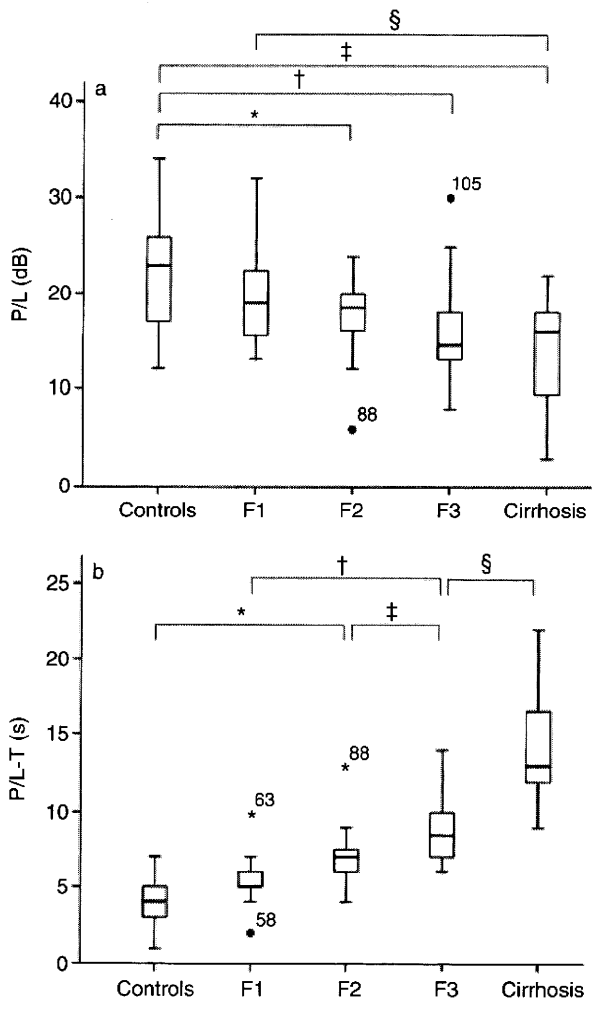

Fig. 5. Maximum intensity ratio between the right portal vein and liver parenchyma and time interval from the onset of contrast enhancement in the right portal vein to the time of the maximum intensity ratio in relation to the grade of hepatic fibrosis. (a) Maximum intensity ratio between the right portal vein and liver parenchyma (dB): significant differences were found between controls and F2 (*$P = 0.0219$), controls and F3 (†$P = 0.0005$), controls and cirrhosis (‡$P < 0.0001$) and F1 and cirrhosis (§$P = 0.0023$). (b) Time Interval, time interval from the onset of contrast enhancement in the right portal vein to the time of the maximum intensity ratio (s): significant differences were found between controls and F2 ($P = 0.0004$), F1 and F3 ($P < 0.0001$), F2 and F3 ($P = 0.0177$), and F3 and cirrhosis ($P < 0.0001$).

Initial study for the diagnosis of cirrhosis using a US contrast agent was performed by Albrecht *et al.* (18) as a transit time analysis with Levovist® (Schering, Berlin, Germany). Similar studies also have reported the usefulness of the second-generation contrast agent SonoVue® (Bracco, Milan, Italy) to diagnose chronic hepatitis and cirrhosis (19, 20). However, their approach was not satisfactory in differentiating the severity of fibrosis in chronic liver disease. The authors speculate that there are some limitations in transit time analysis: transit time is influenced by various changes in the intrahepatic circulation in the progress of liver disease as well as the grade of hepatic fibrosis, and transit time includes only the time factor without the distribution factor of microbubble in the liver parenchyma. Against these backgrounds, we hypothesized that increased hepatic resistance caused by fibrosis may affect the inflow haemodynamics of microbubble to the liver, and we focused on the investigation of the microbubble behaviour, from flowing into the liver to its distribution in the hepatic periphery. One of the reasons for the improved diagnostic ability for the degree of hepatic fibrosis may be that we used the parameter time interval from the onset of contrast enhancement in the right portal vein to the time of the maximum intensity ratio', because it reflects microbubble distribution as well as time. There is another advantage in our technique, that is, stable observation for the main branch of the right hepatic artery and portal vein. As viral infection is the most common cause of chronic liver disease in our country, the liver becomes atrophic with deformity, which makes it difficult to observe both the hepatic vein and the hepatic artery on the same scan plane in some cirrhosis patients. Therefore, our methodology was more reasonable than transit time analysis for patients with chronic liver diseases in our country.

With a vibration-induced mechanical wave, transient elastography (FibroScan; Echosens, Paris, France) is attracting considerable attention as a noninvasive tool for the assessment of hepatic fibrosis (25, 26). A recent report by Friedrich-Rust *et al.* (25) provided several lines of evidence to suggest that FibroScan could predict the grade of hepatic fibrosis; the mean AUC for the diagnosis of marked fibrosis, severe fibrosis and cirrhosis were 0.84 (0.82–0.86), 0.89 (0.88–0.91) and 0.94 (0.93–0.95) respectively. However, because the FibroScan is specialized for the assessment of hepatic fibrosis alone, our technique may have an advantage in this regard, because patients with chronic liver disease receive regular US examination for the supervision of hepatocellular carcinoma, and the additional injection of contrast agent may not be so complicated a procedure. Furthermore, the predictive value of our results for the degree of hepatic fibrosis was almost the same as that of FibroScan. In addition, FibroScan is not suitable for patients with ascites, who are clear candidates for our technique. It is expected that the assessment of hepatic fibrosis by contrast-enhanced US could be carried out as an extension of routine US checkup. However, the assessment of liver fibrosis using noncontrast US might be a goal in the management of chronic liver disease.

Several factors may affect the intrahepatic microbubble behaviours involved with hepatic haemodynamics: causes of liver diseases as aetiological factors, and steatosis, ballooning and inflammation as histological factors. At this point, our study included chronic liver diseases with different kinds of causes, viral infection, alcohol abuse, nonalcoholic steatohepatitis, autoimmune

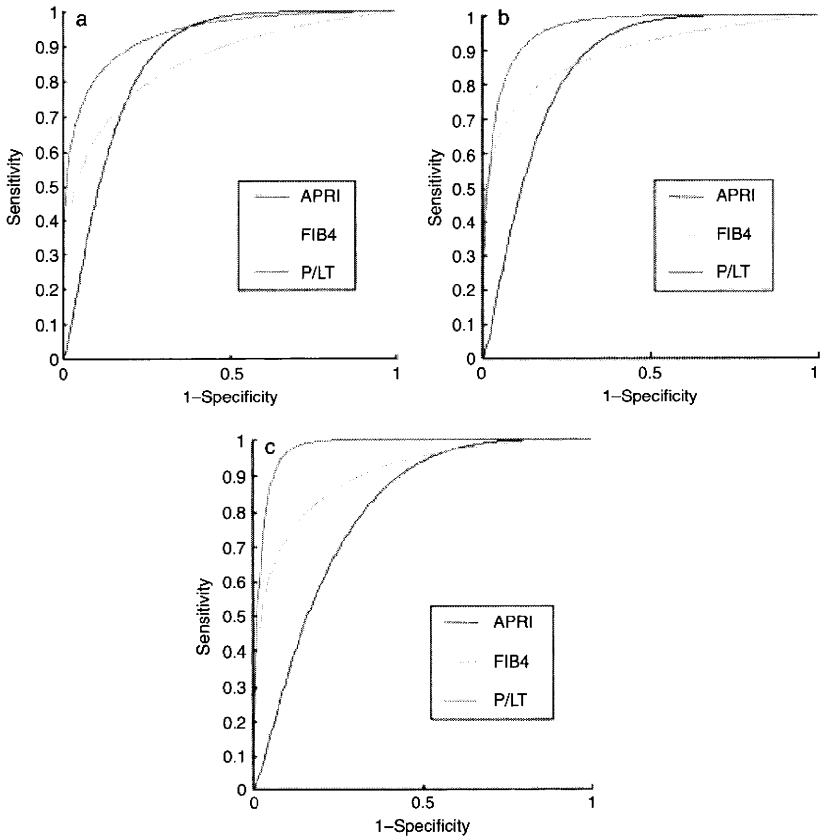

Fig. 6. Receiver operating characteristic curves of time interval from the onset of contrast enhancement in the right portal vein to the time of the maximum intensity ratio, APRI and FIB4. (a) For marked fibrosis (≥F2): AUC values of time interval from the onset of contrast enhancement in the right portal vein to the time of the maximum intensity ratio, APRI, and FIB4 were 0.94, 0.86 and 0.85. (b) For advanced fibrosis (≥F3): AUC values of time interval from the onset of contrast enhancement in the right portal vein to the time of the maximum intensity ratio, APRI, and FIB4 were 0.96, 0.85, and 0.89. (c) For cirrhosis: AUC values of time interval from the onset of contrast enhancement in the right portal vein to the time of the maximum intensity ratio, APRI, and FIB4 were 0.98, 0.80 and 0.90. TI, time interval from the onset of contrast enhancement in the right portal vein to the time of maximum intensity ratio between right portal vein and liver parenchyma.

hepatitis, primary sclerosing cholangitis and cryptogenic, and the patients' population reflects the epidemiology of liver disease in our country. Any kind of chronic liver diseases that met our criteria were included in this study, because our technique aimed at representing the degree of hepatic fibrosis in spite of their different causes. However, as there was a potential bias of patient population in the causes of liver disease, our results presented neither cause-specific validity of contrast-enhanced US with Sonazoid™ to assess the grade of hepatic fibrosis nor relationship between the contrast-enhanced findings and the some pathological factors other than fibrosis, which remain to be solved.

There were some limitations in our study. Firstly, our result was obtained by the observation of only vascular-phase images induced by dynamic microbubble. It is well known that Sonazoid™ has a property of accumulating in the liver, and this is the most important difference between Sonazoid™ and SonoVue® (13–17, 19, 20). In fact, it has not been clarified when intrahepatic microbubble accumulation starts after the agent injection, and whether parenchymal enhancement in vascular phase might be associated with the accumulated microbubble in the liver. However, as contrast enhancement because of circulating microbubble may be dominant in the vascular phase, our study might not utilize fully the potential property of this new contrast agent. SonoVue® without accumulating property in the liver may also be acceptable in this type of study, which should be done in near future. Secondly, our study did not include cases with severe obesity that may limit the US observation, because they are in a relative minority in Japan. The results of the present study should be confirmed in different ethnic groups in different countries. Thirdly, onset time of contrast enhancement was assessed subjectively by visual investigation of recorded images. Although the intensity-based definition of onset time may be reliable, we thought positioning of the region of interest for intensity measurement was not always easy, particularly in the right hepatic artery because of their small caliber.

Liver International (2010)

Therefore, we defined the first frame showing that the arrival of the contrast agent in the vessel was the beginning of the contrast enhancement in this study. The first frame was found in the cine images with frame-by-frame playback, and interobserver variability for the onset of contrast enhancement was quite good. However, our results of the onset time should be confirmed objectively using the digital judgment method, which may be improved in the future.

In conclusion, we observed the contrast enhancement in the liver for 1 min after the injection of Sonazoid™, and found that time interval between the onset of contrast enhancement in the right portal vein and the time of maximum intensity ratio between the intrahepatic right portal vein and liver parenchyma was correlated significantly with the degree of hepatic fibrosis by the quantitative analysis of Sonazoid™-induced sonograms. Although this technique does not allow direct observation of hepatic fibrosis, it may be promising as an indirect evaluation tool for hepatic fibrosis.

References

1. Tandon P, Garcia-Tsao G. Portal hypertension and hepatocellular carcinoma: prognosis and beyond. *Clin Gastroenterol Hepatol* 2006; **4**: 1318–9.
2. Nissen NN, Martin P. Hepatocellular carcinoma: the high-risk patient. *J Clin Gastroenterol* 2002; **35**: S79–85.
3. Williams R. Global challenges in liver disease. *Hepatology* 2006; **44**: 521–6.
4. Desmet VJ, Gerber M, Hoofnagle JH, Manns M, Scheuer PJ. Classification of chronic hepatitis: diagnosis, grading and staging. *Hepatology* 1994; **19**: 1513–20.
5. Poynard T, Ratziu V, Benmanov Y, *et al.* Fibrosis in patients with chronic hepatitis C: detection and significance. *Semin Liver Dis* 2000; **20**: 47–55.
6. Bravo AA, Sheth SG, Chopra S. Liver biopsy. *N Engl J Med* 2001; **344**: 495–500.
7. Scheuer PJ. Liver biopsy in chronic hepatitis: 1968–78. *Gut* 1978; **19**: 554–7.
8. Bedossa P, Dargere D, Paradis V. Sampling variability of liver fibrosis in chronic hepatitis C. *Hepatology* 2003; **38**: 1449–57.
9. Bonekamp S, Kamel I, Solga S, Clark J. Can imaging modalities diagnose and stage hepatic fibrosis and cirrhosis accurately? *J Hepatol* 2009; **50**: 17–35.
10. Gaiani S, Gramantieri L, Venturoli N, *et al.* What is the criterion for differentiating chronic hepatitis from compensated cirrhosis? A prospective study comparing ultrasonography and percutaneous liver biopsy. *J Hepatol* 1997; **27**: 979–85.
11. Schuppan D, Afdhal NH. Liver cirrhosis. *Lancet* 2008; **371**: 838–51.
12. Oberti F, Valsesia E, Pilette C, *et al.* Noninvasive diagnosis of hepatic fibrosis or cirrhosis. *Gastroenterology* 1997; **113**: 1609–16.
13. Forsberg F, Piccoli CW, Liu JB, *et al.* Hepatic tumor detection: MR imaging and conventional US versus pulse-inversion harmonic US of NC100100 during its reticuloendothelial system-specific phase. *Radiology* 2002; **222**: 824–9.
14. Maruyama H, Matsutani S, Saisho H, *et al.* Extra-low acoustic power harmonic images of the liver with perflutren: novel imaging for real-time observation of liver perfusion. *J Ultrasound Med* 2003; **22**: 931–8.
15. Marelli C. Preliminary experience with NC100100, a new ultrasound contrast agent for intravenous injection. *Eur Radiol* 1999; **9**(Suppl. 3): S343–6.
16. Morel DR, Schwieger I, Hohn L, *et al.* Human pharmacokinetics and safety evaluation of SonoVue, a new contrast agent for ultrasound imaging. *Invest Radiol* 2000; **35**: 80–5.
17. Maruyama H, Takahashi M, Ishibashi H, *et al.* Ultrasound-guided treatments under low acoustic power contrast harmonic imaging for hepatocellular carcinomas undetected by B-mode ultrasonography. *Liver Int* 2009; **29**: 708–14.
18. Albrecht T, Blomley MJ, Cosgrove DO, *et al.* Non-invasive diagnosis of hepatic cirrhosis by transit-time analysis of an ultrasound contrast agent. *Lancet* 1999; **353**: 1579–83.
19. Lim AK, Patel N, Eckersley RJ, *et al.* Hepatic vein transit time of SonoVue: a comparative study with Levovist. *Radiology* 2006; **240**: 130–5.
20. Staub F, Tournoux-Facon C, Roumy J, *et al.* Liver fibrosis staging with contrast-enhanced ultrasonography: prospective multicenter study compared with METAVIR scoring. *Eur Radiol* 2009; **19**: 1991–7.
21. Sugimoto H, Kaneko T, Hirota M, Tezel E, Nakao A. Earlier hepatic vein transit-time measured by contrast ultrasonography reflects intrahepatic hemodynamic changes accompanying cirrhosis. *J Hepatol* 2002; **37**: 578–83.
22. Vallet-Pichard A, Mallet V, Nalpas B, *et al.* FIB-4: an inexpensive and accurate marker of fibrosis in HCV infection. Comparison with liver biopsy and fibrotest. *Hepatology* 2007; **46**: 32–6.
23. Metz CE. Receiver operating characteristic analysis: a tool for the quantitative evaluation of observer performance and imaging systems. *J Am Coll Radiol* 2006; **3**: 413–22.
24. Lautt WW. Mechanism and role of intrinsic regulation of hepatic arterial blood flow: hepatic arterial buffer response. *Am J Physiol* 1985; **249**: G549–56.
25. Friedrich-Rust M, Ong MF, Martens S, *et al.* Performance of transient elastography for the staging of liver fibrosis: a meta-analysis. *Gastroenterology* 2008; **134**: 960–74.
26. Wang JH, Changchien CS, Hung CH, *et al.* FibroScan and ultrasonography in the prediction of hepatic fibrosis in patients with chronic viral hepatitis. *J Gastroenterol* 2009; **44**: 439–46.

Bmi1 Promotes Hepatic Stem Cell Expansion and Tumorigenicity in Both *Ink4a/Arf*-Dependent and -Independent Manners in Mice

Tetsuhiro Chiba,[1,2,3*] Atsuyoshi Seki,[1,2*] Ryutaro Aoki,[1,2] Hitoshi Ichikawa,[4] Masamitsu Negishi,[1] Satoru Miyagi,[1] Hideyuki Oguro,[1] Atsunori Saraya,[1] Akihide Kamiya,[5] Hiromitsu Nakauchi,[5] Osamu Yokosuka,[2] and Atsushi Iwama[1,3]

We previously reported that forced expression of *Bmi1* (B lymphoma Moloney murine leukemia virus insertion region 1 homolog) in murine hepatic stem/progenitor cells purified from fetal liver enhances their self-renewal and drives cancer initiation. In the present study, we examined the contribution of the *Ink4a/Arf* tumor suppressor gene locus, one of the major targets of *Bmi1*, to stem cell expansion and cancer initiation. *Bmi1*$^{-/-}$ Delta-like protein (Dlk)$^{+}$ hepatic stem/progenitor cells showed de-repression of the *Ink4a/Arf* locus and displayed impaired growth activity. In contrast, *Ink4a/Arf*$^{-/-}$ Dlk^{+} cells gave rise to considerably larger colonies containing a greater number of bipotent cells than wild-type Dlk^{+} cells. Although *Ink4a/Arf*$^{-/-}$ Dlk^{+} cells did not initiate tumors in recipient nonobese diabetic/severe combined immunodeficiency mice, enforced expression of *Bmi1* in *Ink4a/Arf*$^{-/-}$ Dlk^{+} cells further augmented their self-renewal capacity and resulted in tumor formation *in vivo*. Microarray analyses successfully identified five down-regulated genes as candidate downstream targets for Bmi1 in hepatic stem/progenitor cells. Of these genes, enforced expression of *sex determining region Y-box 17* (*Sox17*) in Dlk^{+} cells strongly suppressed colony propagation and tumor growth. *Conclusion:* These results indicate that repression of targets of Bmi1 other than the *Ink4a/Arf* locus plays a crucial role in the oncogenic transformation of hepatic stem/progenitor cells. Functional analyses of Bmi1 target genes would be of importance to elucidate the molecular machinery underlying hepatic stem cell system and explore therapeutic approaches for the eradication of liver cancer stem cells. (HEPATOLOGY 2010;52:1111-1123)

Abbreviations: Alb, albumin; Bmi1, B lymphoma Moloney murine leukemia virus insertion region 1 homolog; CDK, cyclin-dependent kinase; ChIP, chromatin immunoprecipitation; CK7, cytokeratin 7; DDC, 3,5-diethoxycarbonyl-1,4-dihydrocollidine; Dlk, delta-like protein; EGFP, enhanced green fluorescent protein; ESC, embryonic stem cell; GO, Gene Ontology; H2Aub1, monoubiquitinylated histones H2A; HCC, hepatocellular carcinoma; HSC, hematopoietic stem cell; KO, Kusabira-Orange; MACS, magnetic activated cell sorting; NOD/SCID, nonobese diabetic/severe combined immunodeficiency; NSC, neural stem cell; PcG, polycomb group; PRC, polycomb repressive complex; Rb, retinoblastoma protein; RT-PCR, reverse transcription polymerase chain reaction; Sox17, sex determining region Y-box 17.

From the [1]Department of Cellular and Molecular Medicine and [2]Department of Medicine and Clinical Oncology, Graduate School of Medicine, Chiba University, Chiba, Japan; [3]Japan Science and Technology Corporation, Core Research for Evolutional Science and Technology (JST-CREST), Tokyo, Japan; [4]Genetics Division, National Cancer Center Research Institute, Tokyo, Japan; and [5]Division of Stem Cell Therapy, Center for Stem Cell and Regenerative Medicine, Institute of Medical Science, The University of Tokyo, Tokyo, Japan.

Received April 19, 2010; accepted May 31, 2010.

**These authors contributed equally to this work.*

This work was supported in part by grants for Global COE program (Global Center for Education and Research in Immune System Regulation and Treatment) from the Ministry of Education, Culture, Sports, Science and Technology, Japan, and grants from the Chiba Serum Institute Memorial Fund for Health Medical Welfare, Core Research for Evolutional Science and Technology (CREST) of Japan Science and Technology Corporation (JST), the Takeda Science Foundation, and the Uehara Memorial Foundation.

Address reprint requests to: Atsushi Iwama, Department of Cellular and Molecular Medicine, Graduate School of Medicine, Chiba University, 1-8-1 Inohana, Chuo ward, Chiba 260-8670, Japan. E-mail: aiwama@faculty.chiba-u.jp; fax: +81-43-2262191.

View this article online at wileyonlinelibrary.com.

DOI 10.1002/hep.23793

Potential conflict of interest: Nothing to report.

Additional Supporting Information may be found in the online version of this article.

Polycomb group (PcG) proteins operate as the cellular memory machinery through epigenetic chromatin modifications and are indispensable to the maintenance of cellular identity.[1,2] In particular, Bmi1, a core molecule of polycomb repressive complex 1 (PRC1), plays an important role in the self-renewal of various stem cell systems, including hepatic stem cells.[3]

Recent evidence obtained using stem cell biology–based approaches implies that a rare population of cells in tumors, termed cancer stem cells, possess extreme tumorigenic potential and share several distinctive molecular mechanisms concerning self-renewal, differentiation, and proliferation.[2,4] Of note, it has been demonstrated that Bmi1 is necessary for the maintenance of not only leukemic stem cells but also cancer stem cells in solid tumors.[5,6] Considering that high expression levels of Bmi1 are reported in a wide range of malignancies, Bmi1 could be a general regulator of cancer stem cells as in normal stem cells.

Disruption of the tightly regulated self-renewal process is considered a key early event in carcinogenesis.[7] Enhancement or reacquisition of the self-renewal capability in hematopoietic stem or progenitor cells is essential for leukemogenesis.[8] We also showed that forced expression of *Bmi1* accelerated the self-renewal of hepatic stem/progenitor cells and eventually induced their transformation in an *in vivo* transplant model.[3] However, the molecular machinery underlying the Bmi1-mediated transformation of hepatic stem/progenitor cells remains unclear.

The *Ink4a/Arf* locus, which encodes a cyclin-dependent kinase (CDK) inhibitor, $p16^{Ink4a}$, and a tumor suppressor, $p19^{Arf}$, is a pivotal target of Bmi1.[9] We showed that de-repressed $p16^{Ink4a}$ and $p19^{Arf}$ expression in *Bmi1*-deficient mice was tightly associated with a loss of self-renewing hematopoietic stem cells (HSCs). Deletion of both the *Ink4a* and *Arf* genes substantially restored the self-renewal capacity of *Bmi1*-deficient HSCs. Bmi1 thus regulates HSCs by acting as a critical failsafe against the $p16^{Ink4a}$ and $p19^{Arf}$-dependent senescence pathway.[10,11] Deletion of *Ink4a/Arf* similarly rescues neural stem cell (NSC) self-renewal and frequencies in *Bmi1*-deficient mice, although its effect is reportedly partial.[12] In the oncogenic setting, the Ink4a–retinoblastoma protein (Rb) and Arf-p53 cellular senescence pathways trigger oncogene-induced senescence to eliminate transforming cells that potentially develop into cancer stem cells.[2] Given that enhanced expression of *BMI1* and reduced expression of *INK4A/ARF* are frequently observed in human hepatocellular carcinoma (HCC) samples,[13,14] it would be of importance to understand the contribution of the *Ink4a/Arf* locus to the oncogenic functions of Bmi1 in cancer and search for as-yet-unknown target genes of Bmi1 other than *Ink4a/Arf*.

In the present study, we prepared hepatic stem/progenitor cells from fetal livers of *Bmi1*-deficient and *Ink4a/Arf*-deficient mice and characterized their self-renewal capacity and effects of *Bmi1* overexpression on them. Through these analyses, we found that the *Ink4a/Arf*-independent function of Bmi1 is also essential for its full oncogenic activity in hepatic stem/progenitor cells. Our microarray screening successfully identified candidate downstream targets for Bmi1 in hepatic stem/progenitor cells.

Materials and Methods

Mice. $Bmi1^{+/-}$ mice[15] and $Ink4a\text{-}Arf^{+/-}$ mice (Strain code 01XB1) obtained from Mouse Models of Human Cancers Consortium in the National Cancer Institute (NCI, Frederick, MD) in the C57BL/6 background were used. Nonobese diabetic/severe combined immunodeficient (NOD/SCID) mice were purchased from Sankyo Laboratory (Tsukuba, Japan). All experiments using these mice were performed in accordance with our institutional guidelines for the use of laboratory animals.

Oligonucleotide Array Analysis. Biotin-labeled complementary RNA was prepared with a two-cycle complementary DNA synthesis kit (Affymetrix, Santa Clara, CA) from purified total RNA equivalent to 10,000 cells, and was hybridized to an Affymetrix GeneChip Mouse Genome 430 2.0 array (Affymetrix). The array images were scanned using Affymetrix GeneChip Scanner 3000 7G. The expression value (Signal) for each probe set was calculated using GeneChip Operating Software version 1.4 (Affymetrix). The change value (Signal Log Ratio) and change call (Increase, Marginal Increase, No Change, Marginal Decrease, or Decrease) for each probe set were calculated. Data were obtained for quadrant samples from four independent experiments. To identify differentially expressed genes, we selected probe sets that presented a change call of Increase and a Signal Log Ratio value of ≥ 1 ($\geq$twofold up-regulation) or a change call of Decrease and a Signal Log Ratio value of ≤ -1 ($\geq$twofold down-regulation) in more than three experiments. Moreover, the Welch t test or paired t test was performed to determine significance. Gene Ontology (GO) annotations were performed using the GeneSpring annotation tool (Agilent Technologies, Santa Clara, CA). Microarray data are available at

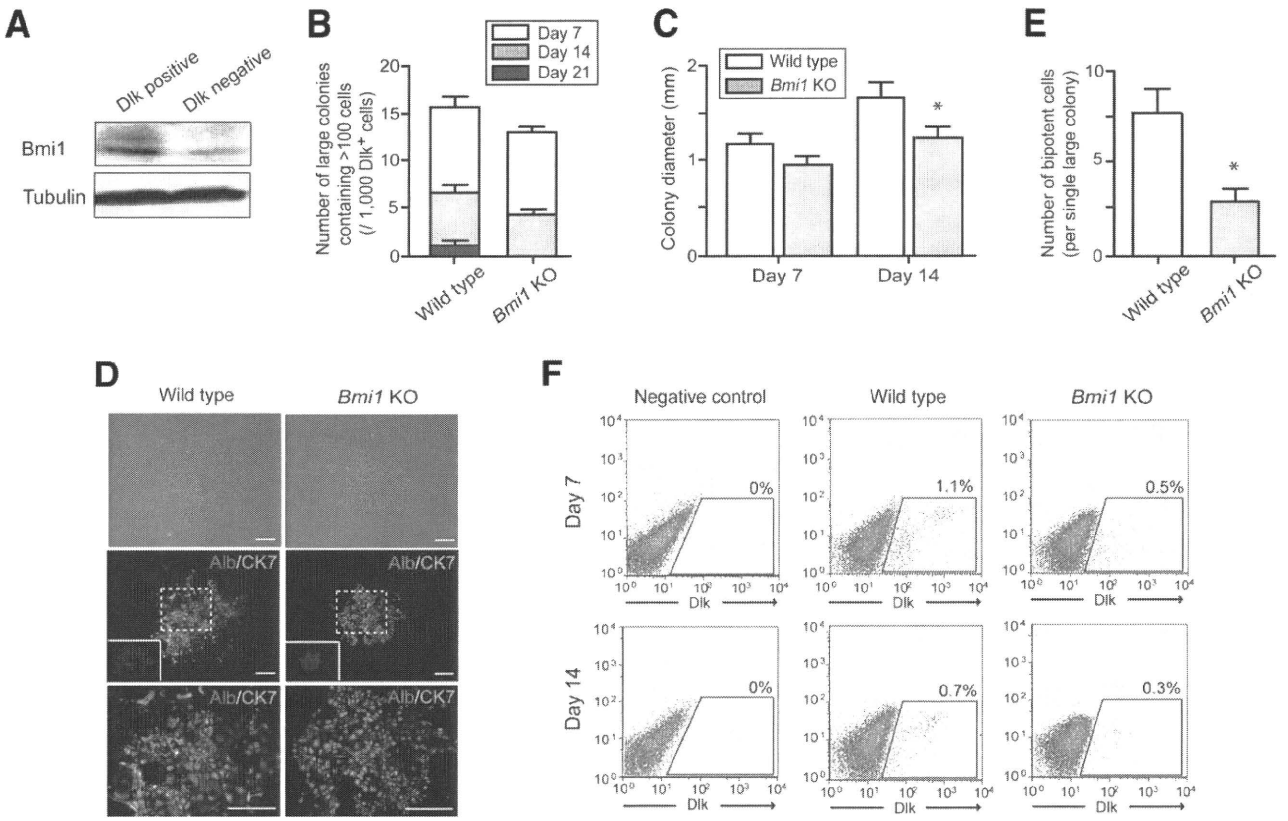

Fig. 1. Colony assays of *Bmi1*$^{-/-}$ hepatic stem cells. (A) Western blot analysis of Bmi1 expression in Dlk^{+} and Dlk^{-} cells purified from wild-type fetal liver. Tubulin was used as a loading control. (B) The number of large colonies containing more than 100 cells at day 7 of culture was traced up to day 21. (C) Colony diameter at days 7 and 14 of culture. *Statistically significant ($P < 0.05$). (D) Bright-field images and immunocytochemical analyses of colonies at day 7 of culture. Alb (red) and CK7 (green) expression was merged. Nuclear DAPI staining (blue) is shown in the insets. (E) The absolute number of Alb^{+}CK7^{+} bipotent cells in large colonies derived from wild-type or *Bmi1*$^{-/-}$ Dlk^{+} cells at day 7 of culture. *Statistically significant ($P < 0.05$). (F) Flow cytometric profiles of colonies derived from wild-type or *Bmi1*$^{-/-}$ Dlk^{+} cells at days 7 and 14 of culture. The percentages of Dlk^{+} cells are shown as mean values for three independent analyses.

http://www.ncbi.nlm.nih.gov/geo/ (accession number: GSE17462).

Other methods are shown in Supporting Materials and Methods.

Results

Impaired Colony Propagation of Bmi1*$^{-/-}$ *Hepatic Stem Cells. Similar to the hematopoietic components, the hepatic components developed normally in *Bmi1*$^{-/-}$ fetal livers and we could recover a comparable number of delta-like protein (Dlk)$^{+}$ hepatic stem/progenitor cells from them. Western blot analysis showed a higher level of Bmi1 expression in wild-type Dlk^{+} cells than Dlk^{-} cells (Fig. 1A). To gain an insight into the role of Bmi1 in hepatic stem cells, we conducted colony assays of wild-type and *Bmi1*$^{-/-}$ Dlk^{+} cells purified by magnetic activated cell sorting (MACS). Flow cytometric analysis revealed that the purity of the sorted Dlk^{+} cells was greater than 90% (Supporting Fig. 1). Approximately 1.5% of wild-type Dlk^{+} cells gave rise to large colonies (consisting of >100 cells) at day 7 of culture. Only a portion of the day 7 colonies kept growing and could be detected as large colonies at days 14 and 21, whereas the majority of colonies stopped expanding and disappeared by days 14 and 21 (Fig. 1B). Although the total number of large colonies did not differ significantly between wild-type and *Bmi1*$^{-/-}$ Dlk^{+} cells at day 7 of culture (Fig. 1B), the diameter of colonies derived from *Bmi1*$^{-/-}$ Dlk^{+} cells was slightly reduced (Fig. 1C). The impeded expansion of *Bmi1*$^{-/-}$ Dlk^{+} cell-derived colonies was obvious at day 14 of culture (Fig. 1B,C). Approximately 10% of large colonies from wild-type Dlk^{+} cells continued to proliferate up to day 21 of culture, whereas no colonies derived from *Bmi1*$^{-/-}$ Dlk^{+} cells expanded beyond day 21 (Fig. 1B).

It has been reported that Dlk^{+} cells are composed of albumin (Alb)$^{+}$ cytokeratin 7 (CK7)$^{+}$ cells and Alb^{+}CK7^{-} cells, and Alb^{+}CK7^{+} cells mainly contribute to the regeneration in retrorsine-treated liver.[16,17] These findings suggest that Alb^{+}CK7^{+} cells, which

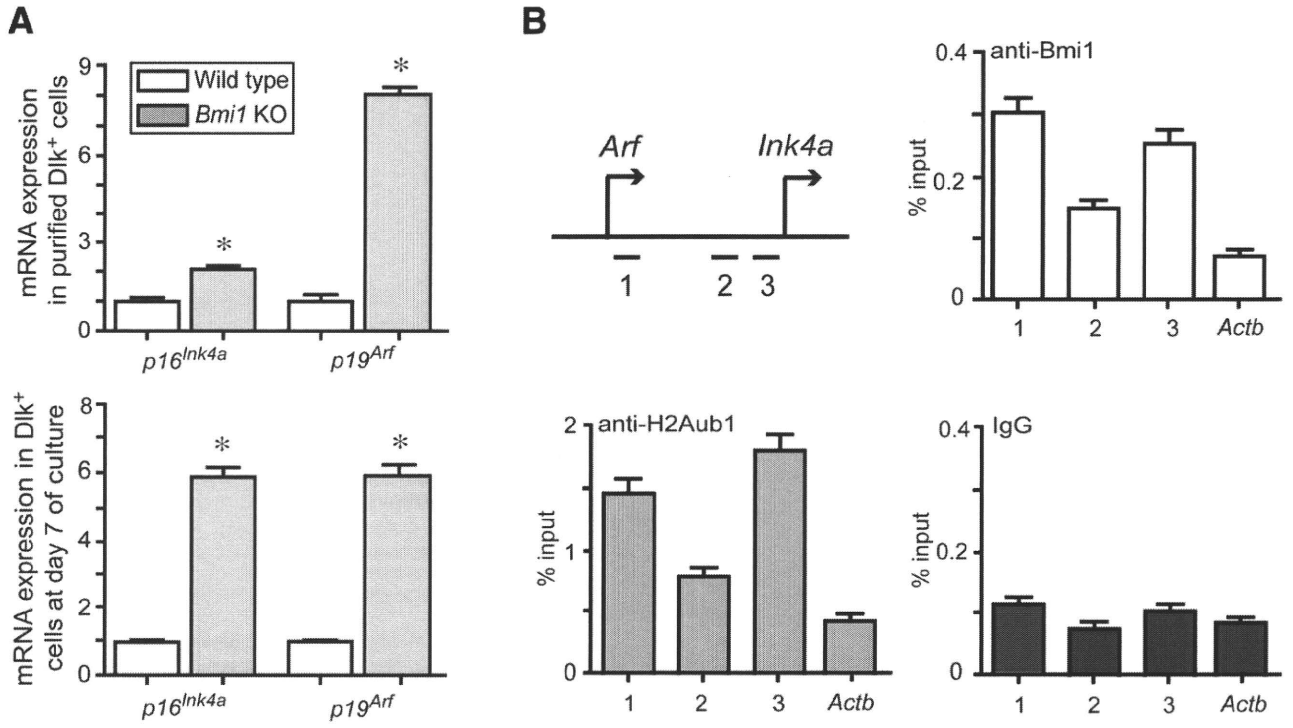

Fig. 2. Regulation of *Ink4a/Arf* expression by *Bmi1*. (A) Real-time RT-PCR analyses of the $p16^{Ink4a}$ and $p19^{Arf}$ genes in freshly purified Dlk^+ cells and Dlk^+ cells cultured for 7 days. *Statistically significant ($P < 0.05$). (B) ChIP analyses of Dlk^+ cells freshly purified from wild-type fetal livers were performed on the *Ink4a/Arf* locus (primer sets 1-3) and the *β-actin* (*Actb*) control promoter region using indicated antibodies. IgG, immunoglobulin G; mRNA, messenger RNA.

have the capacity to give rise to both Alb^+CK7^- and Alb^-Ck7^+ progenies, function as hepatic stem/progenitor cells. Therefore, the quantification of Alb^+CK7^+ impotent cells is one of the approaches to evaluate the content of hepatic stem/progenitor cells, although not all Alb^+CK7^+ cells necessarily have the capacity for bipotential differentiation. Immunocytochemical analyses revealed that the ability of $Bmi1^{-/-}$ Dlk^+ cells to differentiate into Alb^+ hepatocytes and $CK7^+$ cholangiocytes was preserved (Fig. 1D). However, the absolute number of Alb^+CK7^+ bipotent cells were significantly decreased in large colonies derived from $Bmi1^{-/-}$ Dlk^+ cells compared to those in wild-type large colonies (Fig. 1D,E). The absolute number of Alb^+CK7^+ cells per each large colony was 7.6 ± 1.5 and 2.8 ± 0.4, respectively ($P < 0.05$) (Fig. 1E).

Consistent with these findings, flow cytometric analyses demonstrated that the Dlk^+ population in $Bmi1^{-/-}$ colonies decreased rapidly compared to that in wild-type colonies (Fig. 1F). The Dlk^+ fraction in wild-type colonies was 1.1% ± 0.2% at day 7 and 0.7% ± 0.1% at day 14 of culture, whereas that in $Bmi1^{-/-}$ colonies was 0.5% ± 0.1% and 0.3% ± 0.1%, respectively. Conversely, forced expression of *Bmi1* in wild-type Dlk^+ cells significantly promoted colony expansion (Supporting Fig. 2A-C) and increased the Dlk^+ fraction and number of bipotent cells (Supporting Fig. 2D,E).

Oval cells, although their origin is controversial, have been considered stem/progenitor cells in adult liver.[18] Histological analyses demonstrated a drastic decrease in A6-positive oval cell numbers in 3,5-diethoxycarbonyl-1,4-dihydrocollidine (DDC)-treated $Bmi1^{-/-}$ adult liver (Supporting Fig. 3). Together, these findings suggest that Bmi1 plays an important role in the maintenance and expansion of stem/progenitor cells in both fetal and adult livers.

Transcriptional Regulation of the Ink4a/Arf Gene by Bmi1. To examine whether deletion of *Bmi1* causes de-repression of the *Ink4a* and *Arf* genes as observed in HSCs, we conducted real-time reverse transcription polymerase chain reaction (RT-PCR) analyses (Fig. 2A). As expected, messenger RNA levels of *Ink4a* and *Arf* were 2.1-fold and 8.0-fold higher in freshly purified $Bmi1^{-/-}$ Dlk^+ cells than in wild-type Dlk^+ cells, respectively. Colonies derived from $Bmi1^{-/-}$ Dlk^+ cells also showed increased (5.8-fold greater) expression compared to the wild-type colonies. To determine whether Bmi1 is involved in transcriptional regulation of the *Ink4a/Arf* locus, we performed chromatin immunoprecipitation (ChIP) assays using wild-type Dlk^+ cells. ChIP assays demonstrated the binding of

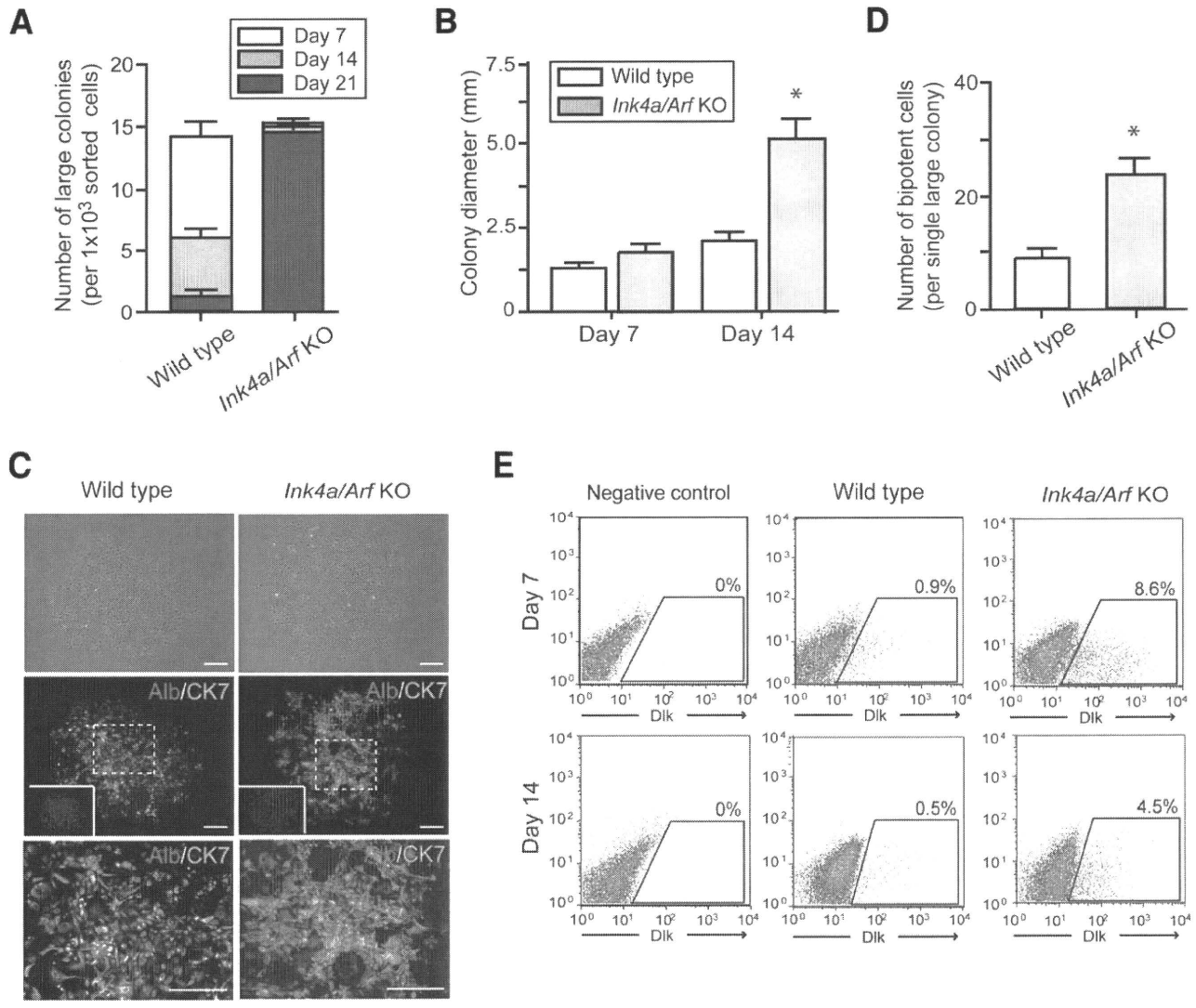

Fig. 3. Colony assays of *Ink4a/Arf*$^{-/-}$ hepatic stem cells. (A) The number of large colonies containing more than 100 cells at day 7 of culture was traced up to day 21. (B) Colony diameter at days 7 and 14 of culture. *Statistically significant ($P < 0.05$). (C) Bright-field images and immunocytochemical analyses of colonies at day 7 of culture. Alb (red) and CK7 (green) expression was merged. Nuclear DAPI staining (blue) is shown in the insets. Scale bar = 200 μm. (D) The absolute number of Alb$^+$CK7$^+$ bipotent cells in large colonies derived from wild-type or *Ink4a/Arf*$^{-/-}$ Dlk$^+$ cells at day 7 of culture. *Statistically significant ($P < 0.05$). (E) Flow cytometric profiles of colonies derived from wild-type or *Ink4a/Arf*$^{-/-}$ Dlk$^+$ cells at days 7 and 14 of culture. The percentages of Dlk$^+$ cells are shown as mean values for three independent analyses.

Bmi1 to the *Ink4a/Arf* locus and increased levels of monoubiquitinylated histone H2A (H2Aub1) (Fig. 2B).

Augmented Colony-Forming Activity of Ink4a/Arf*$^{-/-}$ *Hepatic Stem Cells. To understand the role of the *Ink4a* and *Arf* genes in hepatic stem cells, we next analyzed *Ink4a/Arf*$^{-/-}$ Dlk$^+$ cells in culture. In clear contrast with *Bmi1*$^{-/-}$ Dlk$^+$ cells, *Ink4a/Arf*$^{-/-}$ Dlk$^+$ cells showed pronounced growth activity in culture. The number of large colonies (consisting of more than 100 cells) derived from *Ink4a/Arf*$^{-/-}$ Dlk$^+$ cells was significantly increased compared to that derived from wild-type Dlk$^+$ cells (Fig. 3A,B). By day 14 of culture, *Ink4a/Arf*$^{-/-}$ Dlk$^+$ cells gave rise to distinctly abnormal and large colonies compared to wild-type Dlk$^+$ cells (Fig. 3B,C). More than 95% of large colonies from *Ink4a/Arf*$^{-/-}$ Dlk$^+$ cells further expanded beyond day 21 of culture, although wild-type colonies barely maintained their growth activity (Fig. 3A). Immunocytochemical analyses showed an increase in the proportion and number of Alb$^+$CK7$^+$ bipotent cells in colonies derived from *Ink4a/Arf*$^{-/-}$ Dlk$^+$ cells, particularly in their central area (Fig. 3C). The absolute number of bipotent cells in large colonies derived from wild-type and *Ink4a/Arf*$^{-/-}$ Dlk$^+$ cells at day 7 of culture was 8.2 $\pm$ 2.3 versus 22.7 $\pm$ 4.6 ($P < 0.05$) (Fig.

3D). Flow cytometric analyses revealed that the percentage of Dlk^+ cells in wild-type colonies was 0.9% ± 0.2% at day 7 and 0.5% ± 0.1% at day 14 of culture, although that in *Ink4a/Arf*$^{-/-}$ colonies was 8.6% ± 0.7% and 4.5% ± 0.3%, respectively (Fig. 3E). These findings indicate the enhanced self-renewal capability of hepatic stem cells on the loss of *Ink4a/Arf* expression. Of note, messenger RNA expression of *Bmi1* was comparable between wild-type and *Ink4a/Arf*$^{-/-}$ Dlk^+ cells (data not shown).

As expected, but importantly, the ability of wild-type Dlk^+ cells to propagate colonies was extremely compromised by cotransduction with *Ink4a* and *Arf* retroviruses. Immunocytochemical analyses and flow cytometric analyses showed that the Dlk^+ fraction and bipotent cells were significantly reduced in culture (Supporting Fig. 4).

Enhanced Self-Renewal of Ink4a/Arf*$^{-/-}$ *Hepatic Stem Cells by Bmi1 Overexpression. We previously reported that forced expression of *Bmi1* enhances the self-renewal capacity of hepatic stem/progenitor cells and eventually induces their transformation.[3] To elucidate whether the functional significance of Bmi1 is attributable to the repression of *Ink4a/Arf*, we performed gain-of-function assays of *Bmi1* in *Ink4a/Arf*$^{-/-}$ cells. *Ink4a/Arf*$^{-/-}$ Dlk^+ cells were transduced with either control enhanced green fluorescent protein (*EGFP*) or *Bmi1* 12-18 hours after purification. Enforced expression of Bmi1 was verified by western blot analysis (Fig. 4A). Exogenous Bmi1 in *Ink4a/Arf*$^{-/-}$ Dlk^+ cells did not significantly increase colony number (Fig. 4B). Of note, however, the diameter of *Bmi1*-overexpressing colonies was significantly larger than that of the control colonies (Fig. 4C). Furthermore, flow cytometric analyses showed that the percentage of *Ink4a/Arf*$^{-/-}$ Dlk^+ cells labeled with EGFP was higher in *Bmi1* cultures than in control cultures (22.6% ± 2.3%, 14.0% ± 1.2%, and 8.8% ± 0.7% versus 8.4% ± 1.1%, 3.4% ± 0.5%, and 2.1% ± 0.2% at days 7, 14, and 28 of culture, respectively) (Fig. 4D).

We next carried out single-cell sorting of Dlk^+ cells contained in primary colonies at days 14 and 28 of culture in order to evaluate their self-renewal capacity in terms of replating activity. Dlk^+ cells overexpressing *Bmi1* gave rise to 3.1-fold to 4.0-fold more secondary colonies than the control (Fig. 5A). Secondary colonies were generated in a similar fashion to the original colonies. Immunocytochemical analyses demonstrated that the frequency of Alb^+CK7^+ bipotent cells was significantly higher in secondary colonies derived from Dlk^+ cells collected from the primary *Bmi1*-transduced *Ink4a/Arf*$^{-/-}$ colonies at days 14 and 28 of culture (Fig. 5B,C).

In contrast, *Bmi1*$^{-/-}$*Ink4a/Arf*$^{-/-}$ Dlk^+ cells behaved like *Ink4a/Arf*$^{-/-}$ Dlk^+ cells (Supporting Fig. 5). Although loss of Bmi1 still affected the function of *Ink4a/Arf*$^{-/-}$ hepatic stem/progenitor cells to some extent, these findings indicate that *Ink4a/Arf* is the major target of Bmi1 in hepatic stem cells as in HSCs and NSCs.

Acquisition of Tumorigenic Capacity by Bmi1-Transduced Ink4a/Arf*$^{-/-}$ *Hepatic Stem Cells. We then tested whether the loss of both *Ink4a* and *Arf* is enough for the transformation of hepatic stem cells. Considering that a large number of cells were necessary for transplantations assays, these cells were allowed to form colonies in culture for 28 days. Immunocytochemical analyses showed that more than 90% of cells transduced with *Bmi1* expressed both EGFP, a marker antigen for retrovirus integration, and Flag-tagged Bmi1 (Supporting Fig. 6). Subsequently, a total of 2×10^6 transduced cells were transplanted into the subcutaneous space of NOD/SCID mice (Fig. 5D). Although all the mice transplanted with *Bmi1*-transduced *Ink4a/Arf*$^{-/-}$ Dlk^+ cells developed tumors, none of those transplanted with control *Ink4a/Arf*$^{-/-}$ Dlk^+ cells did. Histological analyses revealed that the subcutaneous tumors consisted of both Alb^+ parenchymal cells and a $CK7^+$ glandular structure (Fig. 5D). The histological finding is consistent with our previous observation in tumors derived from *Bmi1*-transduced wild-type hepatic stem cells.[3] These findings clearly indicate that repression of the *Ink4a* and *Arf* genes is not enough for Bmi1 to achieve its tumorigenic potential in hepatic stem cells.

Gene Expression Analyses of Bmi1-Transduced Ink4a/Arf*$^{-/-}$ *Hepatic Stem Cells. In order to explore novel targets for Bmi1, *Ink4a/Arf*$^{-/-}$ Dlk^+ cells were infected with either the control *EGFP* or *Bmi1*-expressing retrovirus and allowed to form colonies. Dlk^+ cells were purified from colonies at day 28 of culture by cell sorting and subjected to gene expression profiling using oligonucleotide microarrays. We selected genes exhibiting a twofold or greater change with statistical significance in *Bmi1*-transduced *Ink4a/Arf*$^{-/-}$ Dlk^+ cells compared to control *Ink4a/Arf*$^{-/-}$ Dlk^+ cells. As a result, we identified 75 down-regulated genes and 97 up-regulated genes in total (Supporting Table 1). Functional annotation based on GO showed significant enrichment for down-regulated genes which fell into the category "metabolism" and "transport", which included many hepatocyte maturation genes (Fig. 6A). This indicates that Bmi1 strongly suppresses the differentiation and maturation of hepatocytes.

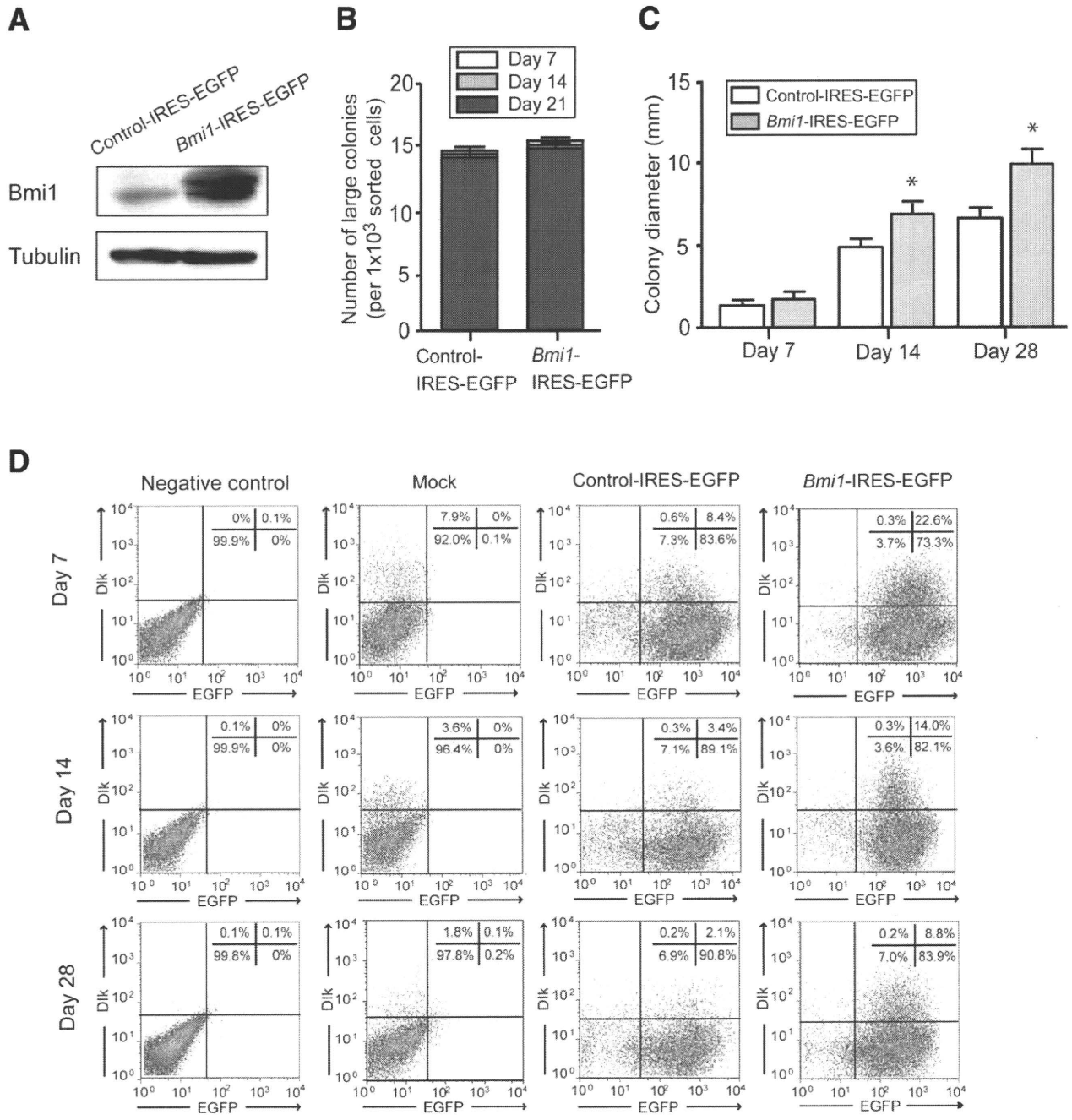

Fig. 4. Gain-of-function assays of *Bmi1* in *Ink4a/Arf*$^{-/-}$ Dlk^{+} cells. (A) Cells transduced with indicated retroviruses were subjected to western blot analysis using anti-Bmi1 and anti-tubulin (loading control) antibodies. (B) The number of large colonies containing more than 100 cells at day 7 of culture was traced up to day 21. (C) The diameter of colonies at days 7, 14, and 28 after transduction of indicated retroviruses. *Statistically significant ($P < 0.05$). (D) Flow cytometric profiles of colonies derived from nontransduced (mock) and *EGFP* or *Bmi1*-transduced *Ink4a/Arf*$^{-/-}$ Dlk^{+} cells at days 7, 14, and 28 in culture. The percentages of each fraction are shown as mean values for three independent analyses.

Recent whole-genome ChIP-on-chip analyses successfully identified genes that are bound by PRC1 and PRC2 complexes in embryonic stem cells (ESCs).[19-21] Boyer et al. reported the genes occupied by PRC1 (Phc1 and Rnf2) and PRC2 (Suz12 and Eed) in murine ESCs.[19] To explore a novel target of Bmi1 in hepatic stem/progenitor cells, we compared the list of down-regulated genes with the ChIP-on-chip data documented by Boyer et al.[19] As a result, five genes namely, *Sox17*, *Irx5*, *Gjb2*, *Shox2*, and *Bhmt2* in the present study appeared to be regulated by both PRC1 and/or PRC2 in ESCs (Fig. 6B). We therefore considered these genes as candidates for direct targets of Bmi1 in hepatic stem cells and performed further analyses on them. In order to confirm the altered expression of these 5 candidate genes, *Ink4a/Arf*$^{-/-}$ Dlk^{+}

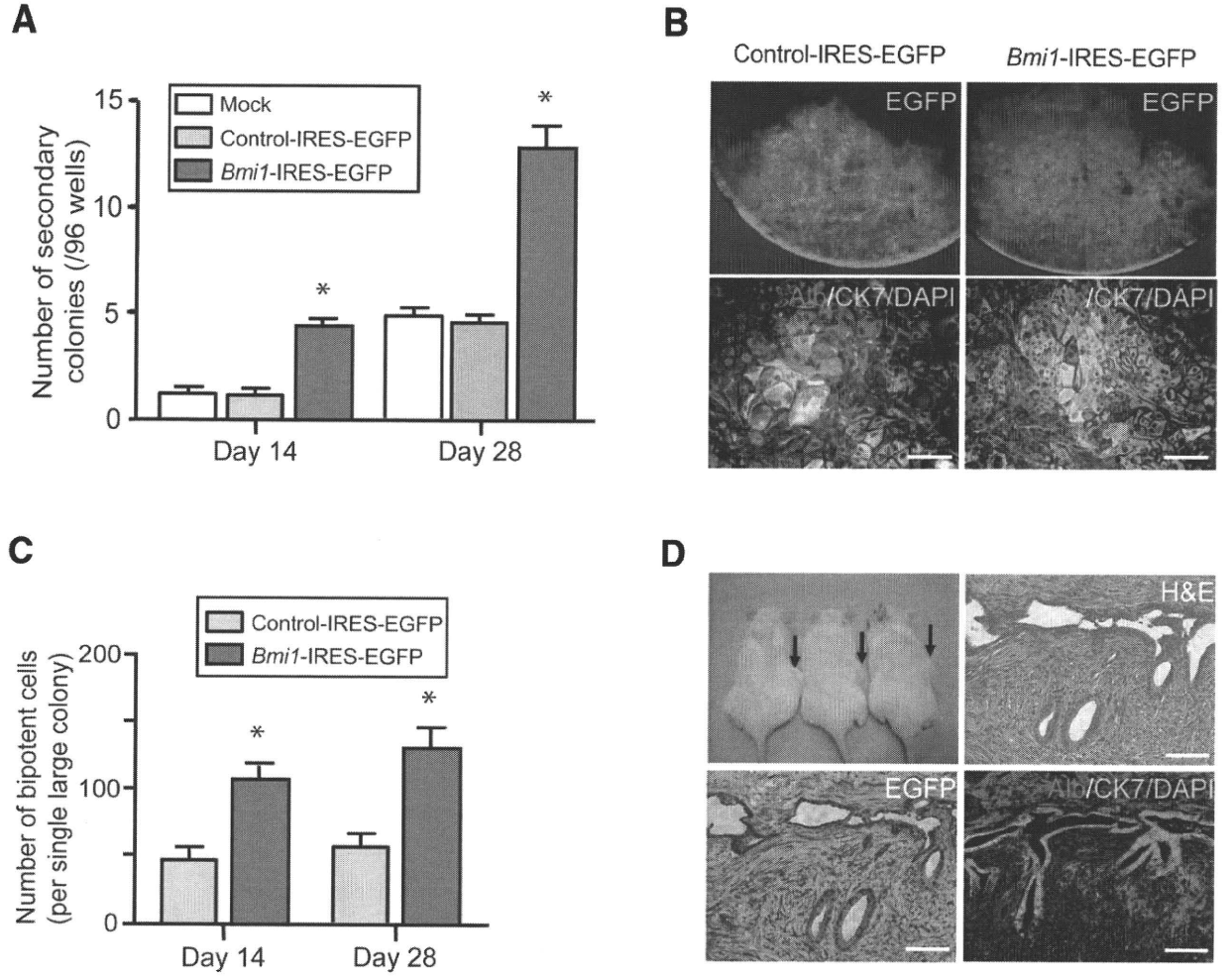

Fig. 5. Replating assays and implantation of *Bmi1*-transduced *Ink4a/Arf*$^{-/-}$ Dlk^{+} cells. (A) Dlk^{+} cells in primary colonies generated from nontransduced (mock) and *EGFP* or *Bmi1*-transduced *Ink4a/Arf*$^{-/-}$ Dlk^{+} cells were clone-sorted at days 14 and 28 of culture and allowed to form colonies. The replating efficiency of Dlk^{+} cells was evaluated by counting the number of secondary colonies containing more than 100 cells 14 days after replating by clone-sorting. *Statistically significant ($P < 0.05$). (B) Fluorescence images (upper panels) and dual immunostaining (lower panels) of secondary clonal colonies derived from *EGFP* or *Bmi1*-transduced *Ink4a/Arf*$^{-/-}$ Dlk^{+} cells at day 28 of culture. Alb (red) and CK7 (green) expression in secondary colonies was merged with nuclear DAPI staining (blue). Scale bar = 100 μm. (C) The absolute number of Alb^{+}CK7^{+} bipotent cells in secondary large colonies at day 14 of subculture. *Statistically significant ($P < 0.05$). (D) *Ink4a/Arf*$^{-/-}$ Dlk^{+} cells were transduced with the control *EGFP* or *Bmi1*-expressing retrovirus and a total of 2×10^{6} transduced cells were transplanted into the subcutaneous space of NOD/SCID mice. *Bmi1*-transduced *Ink4a/Arf*$^{-/-}$ cells formed tumors in the right subcutaneous space of recipient mice (arrows), whereas the same number of control *EGFP*-transduced *Ink4a/Arf*$^{-/-}$ cells did not generate tumors in the left space. Hematoxylin and eosin (H&E) staining of tumors demonstrated histological features compatible with combined hepatocellular and cholangiocellular carcinoma. Immunohistochemical analysis revealed that the tumors were positive for EGFP and consisted of Alb^{+} parenchymal cells (red) and CK7^{+} glandular structures (green). Scale bar = 200 μm.

cells transduced with either control *EGFP* or *Bmi1* were purified from colonies at day 28 of culture and subjected to real-time RT-PCR analyses. The selected five genes exhibited similar expression profiles as in the microarray analysis in *Ink4a/Arf*$^{-/-}$ Dlk^{+} cells (Fig. 6C). Forced expression of *Bmi1* in wild-type Dlk^{+} cells significantly repressed the expression of these genes in a similar fashion to that in *Ink4a/Arf*$^{-/-}$ Dlk^{+} cells (Fig. 6C).

Gain-of-Function Assays of Sox17 in Hepatic Stem Cells. Among candidates for Bmi1 targets, *sex determining region Y-box 17* (*Sox17*) was most severely down-regulated following *Bmi1*-overexpression in hepatic stem cells (Fig. 6C). It has been reported that *Sox17* is highly expressed in the very early definitive endoderm[22] and in hepatocyte-like cells derived from ESCs.[23] These findings prompted us to further examine the role of *Sox17* in hepatic stem cell self-renewal and tumorigenesis. ChIP assays in wild-type Dlk^{+} cells demonstrated specific binding of Bmi1 and an increased level of H2Aub1 at the *Sox17* promoter only in cells transduced with the *Bmi1* retrovirus (Fig. 7A).

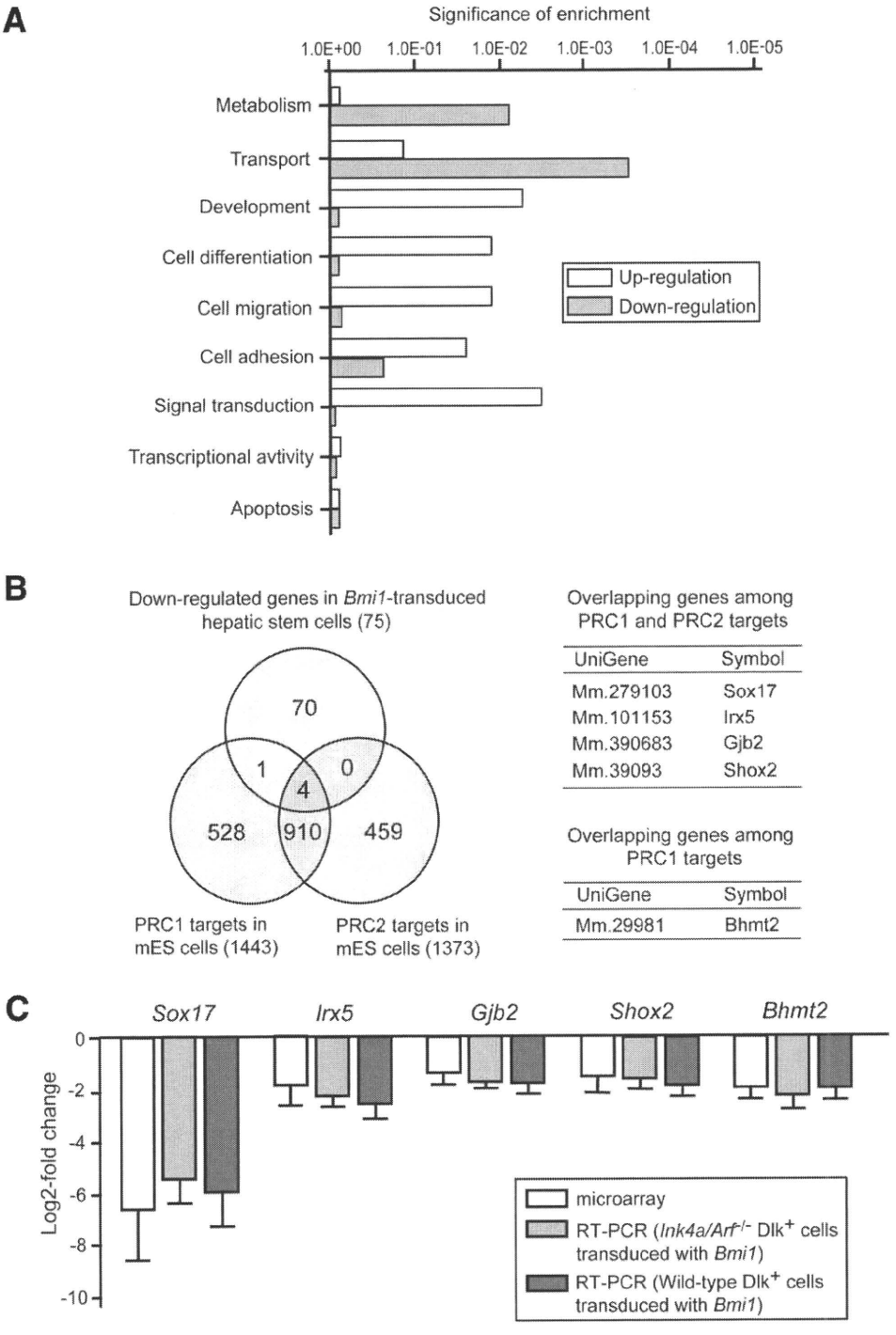

Fig. 6. Gene expression profiles of *Bmi1*-transduced *Ink4a/Arf*$^{-/-}$ Dlk^{+} cells. (A) Gene Ontology (GO) analyses of differentially expressed genes. (B) The overlap of down-regulated genes in the present analysis and PRC targets identified by ChIP-on-chip analyses in mouse ESCs[27] are depicted in a Venn diagram (left panel) and in tables at right. (C) Wild-type and *Ink4a/Arf*$^{-/-}$ Dlk^{+} cells were infected with either the control *EGFP* or *Bmi1*-expressing retrovirus and allowed to form colonies. Dlk^{+} cells were purified from these colonies at day 28 of culture and subjected to real-time RT-PCR analysis. The messenger RNA expression of candidate genes in *Bmi1*-overexpressing cells was compared to that in control cells. The data obtained by microarray analyses are also presented.

All these findings indicate that Bmi1 could directly regulate the expression of *Sox17*.

We next tested the effect of Sox17 in a gain-of-function assay. Overexpression of Sox17 was confirmed by western blotting (Fig. 7B). Enforced expression of *Sox17* in wild-type Dlk^{+} cells severely impaired the formation of colonies and reduced the number as well as size of colonies (Fig. 7C,D). Dlk^{+} cells transduced with *Sox17* did not form any large colonies containing more than 100 cells at day 7 of culture (Fig. 7C) and no colonies expanded beyond day 14 of culture (data not shown). Immunocytochemical analyses showed a decrease in number of Alb^{+}CK7^{+} bipotent cells in colonies derived from Dlk^{+} cells transduced with *Sox17* compared to the control colonies (Fig. 7D,E). Concordant with this, flow cytometric analyses demonstrated that the Dlk^{+} fraction in *Sox17*-transduced colonies was 0.3% ± 0.1%, much lower that that in wild-type colonies (0.9% ± 0.2%) (Fig. 7F).

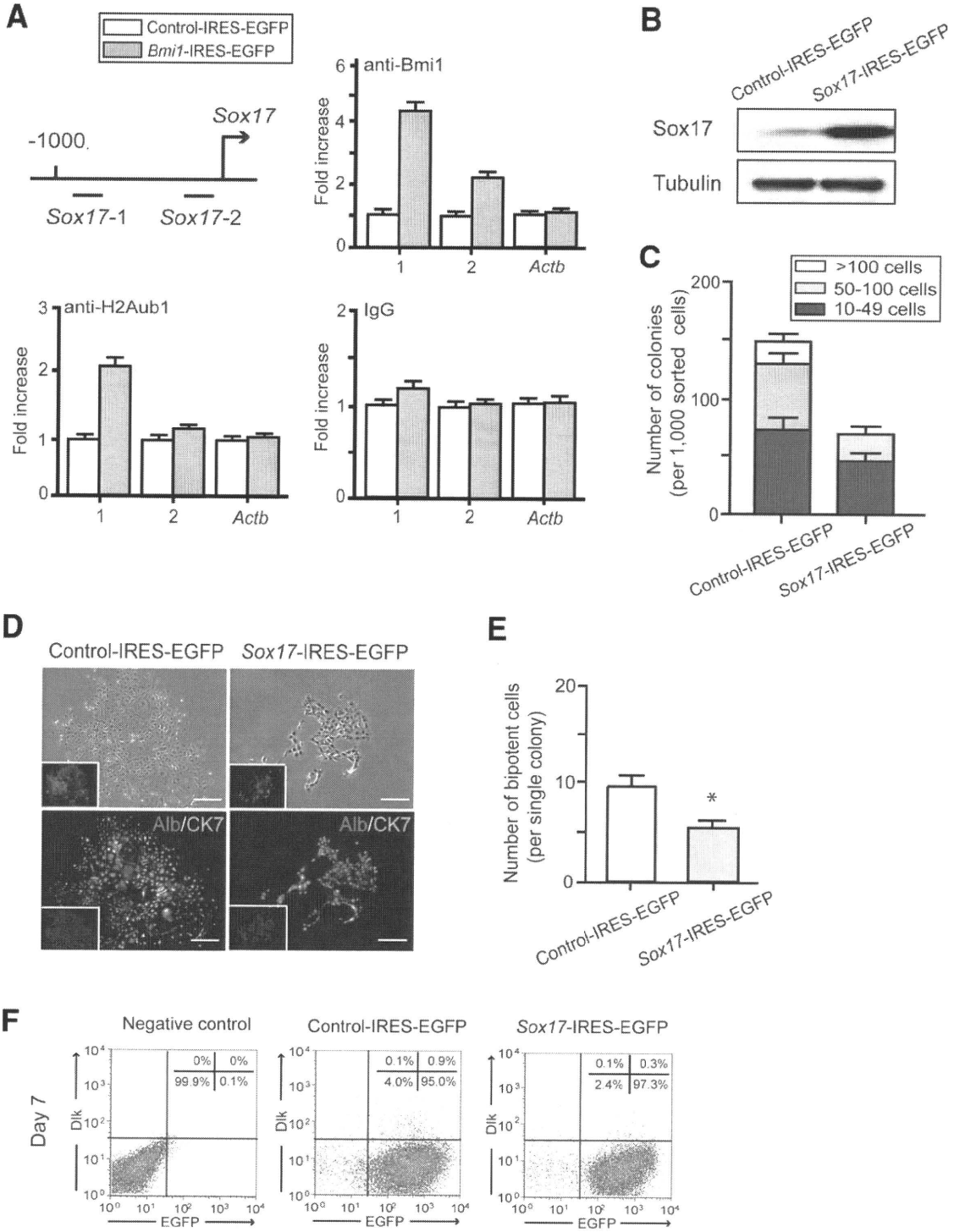

Fig. 7. Gain-of-function assay of *Sox17* in wild-type Dlk$^+$ cells. (A) ChIP analyses of wild-type Dlk$^+$ cells transduced with *EGFP* or *Bmi1* on the *Sox17* locus and *Actb* control promoter region using anti-Bmi1 and anti-H2Aub1 antibodies. *Statistically significant ($P < 0.05$). (B) Western blot analysis in *Sox17*-transduced wild-type Dlk$^+$ cells using anti-Sox17 and anti-tubulin (loading control) antibodies. (C) Enforced expression of *Sox17* in wild-type Dlk$^+$ cells markedly decreased both the total number of colonies and the number of large colonies containing more than 100 cells at day 7 of culture. *Statistically significant ($P < 0.05$). (D) Bright-field images and immunocytochemical analyses of colonies derived from wild-type Dlk$^+$ cells transduced with *Sox17* at day 7 of culture. Alb (red) and CK7 (green) expression was merged. Nuclear DAPI staining (blue) is shown in the insets. Scale bar = 200 μm. (E) The absolute number of Alb$^+$CK7$^+$ bipotent cells in colonies derived from wild-type Dlk$^+$ cells transduced with *Sox17* at day 7 of culture. *Statistically significant ($P < 0.05$). (F) Flow cytometric profiles of colonies derived from *EGFP* or *Sox17*-transduced wild-type Dlk$^+$ cells at day 7 of culture. The percentages of each fraction are shown as mean values for three independent analyses.

To elucidate the impact of *Sox17* on the tumorigenic process driven by *Bmi1*-overexpressing hepatic stem cells, we cotransduced *Ink4a/Arf*$^{-/-}$ Dlk^{+} cells with *Bmi1* and *Sox17*. *Ink4a/Arf*$^{-/-}$ Dlk^{+} cells were simultaneously transduced with *Sox17*-IRES-EGFP and *Bmi1*-IRES-Kusabira-Orange (KO)-expressing retroviral vectors (Supporting Fig. 7A). Flow cytometric profiles demonstrated that more than 90% of cells were successfully cotransduced (Supporting Fig. 7B). A total of 2×10^6 *Ink4a/Arf*$^{-/-}$ cells cotransduced with *Bmi1* and *Sox17* or control *EGFP* were transplanted into the subcutaneous space of NOD/SCID mice. Cotransduction of *Bmi1* and *Sox17* resulted in a significant reduction in tumor volume compared to the cotransduction of *Bmi1* and control *EGFP* (Supporting Fig. 6C). This result indicates that *Sox17* suppresses the tumorigenic activity of *Bmi1*-overexpressing hepatic stem cells.

We then further tested the effect of *Sox17* knockdown in wild-type Dlk^{+} cells (Supporting Fig. 8). *Sox17* knockdown mildly promoted colony expansion and increased the Dlk^{+} fraction and the number of bipotent cells, although its effect was not statistically significant. Transplantation of 2×10^6 *Sox17*-knockdown Dlk^{+} cells did not develop subcutaneous tumors in NOD/SCID mice at all (data not shown).

Discussion

Bmi1, a component of PRC1, regulates the cell cycle, apoptosis and senescence by repressing the *Ink4a/Arf* locus.[5,10] p19^{Arf} suppresses MDM2, which mediates ubiquitin-dependent degradation of p53, and subsequently activates p53 target genes involved in cell cycle arrest and apoptosis, including *p21*.[24] Direct binding of p16^{Ink4a} to CDK4 and CDK6 keeps Rb hypophosphorylated. Hypophosphorylated Rb represses E2F-dependent transcription leading to cell cycle arrest and senescence.[24] Thus, the repression of the *Ink4a/Arf* locus by Bmi1 has a great impact on the maintenance of self-renewing stem cells.

In the present study, *Bmi1*$^{-/-}$ hepatic stem cells showed high levels of *Ink4a* and *Arf* expression and significantly but modestly impaired colony expansion and self-renewal in culture. Although *Bmi1*$^{-/-}$ liver is functionally and histologically normal,[15] oval cell induction following DDC treatment was apparently impaired in *Bmi1*$^{-/-}$ mice (Supporting Fig. 3). Considering the results of gain-of-function (Supporting Fig. 2) and loss-of-function assays of *Bmi1* (Fig. 1), the possibility exists that redundancy among other PcG molecules such as Mel18 weakens the phenotype of *Bmi1*$^{-/-}$ hepatic stem cells in developing and adult liver.[25] In clear contrast, *Ink4a/Arf*$^{-/-}$ hepatic stem cells exhibited enhanced colony formation and retained a large Dlk^{+} population in culture compared to the wild type. Furthermore, deletion of both *Ink4a* and *Arf* largely restored the impaired self-renewal capacity of *Bmi1*$^{-/-}$ hepatic stem cells (Supporting Fig. 5). These findings indicate that *Ink4a/Arf* is the major target of Bmi1 in hepatic stem cells as in HSCs and NSCs.[11,12]

Bmi1 is also essential for cancer stem cells as demonstrated in a mouse leukemia model as well as in a mouse lung tumor model generated by the expression of a mutant K-ras gene in bronchioalveolar stem cells.[5,26] In addition, we previously demonstrated that forced expression of *Bmi1* promotes the self-renewal of hepatic stem/progenitor cells and contributes to malignant transformation.[3] All these findings highlight the important role of Bmi1 in both the development and maintenance of cancer stem cell systems. Of interest, an *Ink4a/Arf*-independent contribution of Bmi1 to not only self-renewal in neural stem cells but also tumorigenesis in a mouse model for glioma has been reported.[27,28] The current *in vivo* transplant assays ascertained that *Bmi1*-transduced *Ink4a/Arf*$^{-/-}$ Dlk^{+} cells but not control *Ink4a/Arf*$^{-/-}$ Dlk^{+} cells acquire tumorigenic potential. *Bmi1*-transduced *Ink4a/Arf*$^{-/-}$ Dlk^{+} cells showed an augmented self-renewal capability as evident from the higher replating efficiency in the single cell-sorting analysis compared to *Ink4a/Arf*$^{-/-}$ Dlk^{+} cells. These results clearly demonstrated that repression of the *Ink4a/Arf* locus only does not directly drive tumor initiation in hepatic stem cells. Considering that *Ink4a/Arf*$^{-/-}$ mice barely developed primary liver tumors in their lifetime,[29] repression of additional targets of *Bmi1* may be needed in cancer initiation.

To evaluate the impact of Bmi1 on gene expression in hepatic stem cells and to explore the additional targets of Bmi1 related to tumorigenesis, we conducted an oligonucleotide array analysis using *Bmi1*-transduced *Ink4a/Arf*$^{-/-}$ Dlk^{+} cells and the control *Ink4a/Arf*$^{-/-}$ Dlk^{+} cells. The screening of more than 39,000 transcripts successfully identified 75 down-regulated and 97 up-regulated genes (Supporting Table 1). As expected, enforced expression of *Bmi1* contributed to the maintenance of stemness features and suppression of differentiation-related genes. The present analysis revealed gene expression to be up-regulated for the hepatic stem cell markers *Prom1* (*CD133*) ($P = 0.041$) and *EpCAM* ($P = 0.017$) and down-regulated for the hepatocyte differentiation markers *Cps1* ($P = 0.010$), Mat1a ($P = 0.011$), and *Gjb2* (*Cx26*) ($P = 0.010$).

Among these, *Mat1a* knockout mice have been reported to be hypersensitive to oxidative stress and developed steatosis and HCC.[30] Furthermore, reduced expression of *Gjb2* (*Cx26*) is known to contribute to the promotion and progression of hepatocarcinogenesis in rats.[31]

Of interest, our microarray analysis unveiled the altered expression of genes involved in Wnt/β-catenin signaling; down-regulation of the Wnt antagonist *Sox17* ($P = 0.009$), up-regulation of a Wnt downstream effector *Cyclin D1* ($P = 0.001$), and modestly increased expression of the Wnt receptor *Fzd7* ($P = 0.098$). Wnt/β-catenin signaling is integrally associated with the regulation of stem cells and development of cancer[32] and activated Wnt/β-catenin signaling promotes the proliferation and transformation of hepatic stem/progenitor cells.[3] Together, these results imply that enforced expression of *Bmi1* results in an enhancement of stemness features and the acquisition of malignant potential in normal hepatic stem/progenitor cells, at least in part, through the activation of Wnt signaling. However, further analysis would be necessary to elucidate the relationship between Bmi1 and Wnt signaling.

Surprisingly but importantly, none of the 75 down-regulated genes following *Bmi1*-overexpression was included among the 305 up-regulated genes in neural progenitor cells after *Bmi1* knockdown.[27] Likewise, there existed no overlapping genes between the current expression profile and the 101 commonly regulated genes following *BMI1* knockdown between medulloblastoma and Ewing sarcoma cells.[33,34] In contrast, we detected several genes down-regulated following *Bmi1*-overexpression in hepatic stem/progenitor cells which are also regulated by Bmi1 in hematopoietic stem/progenitor cells (data not shown). These findings support the fact that PcG proteins function in a cell type-specific manner and the composition of PcG complexes is highly dynamic and differs in different cell-types and even at different gene loci.[35]

A comparison of the down-regulated genes with the ChIP-on-chip data for PcG complexes in ESCs revealed five genes that are regulated by PRC1 in ESCs as potential direct targets of Bmi1 in hepatic stem/progenitor cells (Fig. 6B). One of these genes, *Sox17*, is an endodermal marker gene and *Sox17*$^{-/-}$ mice die in the embryonic stage because the endoderm fails to form properly.[22] Therefore, its role in hepatic stem cells remained obscure. In the present study, self-renewal capacity of hepatic stem cells was inversely correlated with the *Sox17* expression levels. Furthermore, cotransduction of *Sox17* with *Bmi1* repressed tumorigenic capacity of Bmi1 in NOD/SCID mice. These findings suggest that Sox17 acts as a tumor suppressor in a specific type of tumor originating from hepatic stem cells. The finding that it is transcriptionally silenced by DNA methylation in human colon cancer cells further supports its role as a tumor suppressor gene.[36] On the other hand, *Sox17*-knockdown in Dlk$^+$ cells alone did not promote tumor initiation in immunodeficient mice. Tumor initiation usually requires multiple steps including activation of oncogenes and repression of tumor suppressor genes. As a number of candidate genes of Bmi1 were identified in this study, coordinated regulation of multiple Bmi1 targets might be needed to recapitulate Bmi1-mediated tumorigenesis *in vivo*. In this regard, knockdown of *Sox17* or other candidate target genes in *Ink4a/Arf*$^{-/-}$ Dlk$^+$ cells would be intriguing to assess for their tumorigenic activity *in vivo*.

Finally, our findings demonstrated that Bmi1 regulates the self-renewal of hepatic stem/progenitor cells to a large extent through the suppression of *Ink4a/Arf*. However, it is evident that targets of Bmi1 other than the *Ink4a/Arf* locus are also responsible for the development of cancer. Further analyses are necessary to determine the roles of the genes listed here in liver development, regeneration, and cancer.

Acknowledgment: The authors thank Dr. M. van Lohuizen for *Bmi1*$^{+/-}$ mice, Dr. W. Pear for the MIGR1 vector, Dr. Valentina M. Factor for the anti-A6 antibody, Dr. N. Nozaki for the anti-Bmi1 antibody, Dr. A. Miyawaki for Kusabira orange, Y. Yamazaki for technical support with the flow cytometry, and M. Tanemura for laboratory assistance.

References

1. Valk-Lingbeek ME, Bruggeman SWM, van Lohuizen M. Stem cells and cancer: the polycomb connection. Cell 2004;118:409-418.
2. Sparmann A, van Lohuizen M. Polycomb silencers control cell fate, development and cancer. Nat Rev Cancer 2006;6:846-856.
3. Chiba T, Zheng YW, Kita K, Yokosuka O, Saisho H, Onodera M, et al. Enhanced self-renewal capability in hepatic stem/progenitor cells drives cancer initiation. Gastroenterology 2007;133:937-950.
4. Mishra L, Banker T, Murray J, Byers S, Thenappan A, He AR, et al. Liver stem cells and hepatocellular carcinoma. HEPATOLOGY 2009;49:318-329.
5. Lessard J, Sauvageau G. Bmi-1 determines the proliferative capacity of normal and leukaemic stem cells. Nature 2003;423:255-260.
6. Leung C, Lingbeek M, Shakhova O, Liu J, Tanger E, Saremaslani P, et al. Bmi1 is essential for cerebellar development and is overexpressed in human medulloblastomas. Nature 2004;428:337-341.
7. Pardal R, Clarke MF, Morrison SJ. Applying the principles of stem-cell biology to cancer. Nat Rev Cancer 2003;3:895-902.
8. Jamieson CH, Weissman IL, Passegue E. Chronic versus acute myelogenous leukemia: a question of self-renewal. Cancer Cell 2004;6:531-533.

9. Park IK, Morrison SJ, Clarke MF. Bmi1, stem cells, and senescence regulation. J Clin Invest 2004;113:175-179.
10. Iwama A, Oguro H, Negishi M, Kato Y, Morita Y, Tsukui H, et al. Enhanced self-renewal of hematopoietic stem cells mediated by the polycomb gene product Bmi-1. Immunity 2004;21:843-851.
11. Oguro H, Iwama A, Morita Y, Kamijo T, van Lohuizen M, Nakauchi H. Differential impact of Ink4a and Arf on hematopoietic stem cells and their bone marrow microenvironment in Bmi1-deficient mice. J Exp Med 2006;203:2247-2253.
12. Molofsky AV, He S, Bydon M, Morrison SJ, Pardal R. Bmi-1 promotes neural stem cell self-renewal and neural development but not mouse growth and survival by repressing the p16Ink4a and p19Arf senescence pathways. Genes Dev 2005;19:1432-1437.
13. Sasaki M, Ikeda H, Itatsu K, Yamaguchi J, Sawada S, Minato H, et al. The overexpression of polycomb group proteins Bmi1 and EZH2 is associated with the progression and aggressive biological behavior of hepatocellular carcinoma. Lab Invest 2008;88:873-882.
14. Tannapfel A, Busse C, Weinans L, Benicke M, Katalinic A, Geissler F, et al. INK4a-ARF alterations and p53 mutations in hepatocellular carcinomas. Oncogene 2001;20:7104-7109.
15. van der Lugt NM, Domen J, Linders K, van Roon M, Robanus-Maandag E, te Riele H, et al. Posterior transformation, neurological abnormalities, and severe hematopoietic defects in mice with a targeted deletion of the bmi-1 proto-oncogene. Genes Dev 1994;8:757-769.
16. Oertel M, Menthena A, Dabeva MD, Shafritz DA. Cell competition leads to a high level of normal liver reconstitution by transplanted fetal liver stem/progenitor cells. Gastroenterology 2006;130:507-520.
17. Dabeva MD, Petkov PM, Sandhu J, Oren R, Laconi E, Hurston E, et al. Proliferation and differentiation of fetal liver epithelial progenitor cells after transplantation into adult rat liver. Am J Pathol 2000;156:2017-2031.
18. Wang X, Foster M, Al-Dhalimy M, Lagasse E, Finegold M, Grompe M. The origin and liver repopulating capacity of murine oval cells. Proc Natl Acad Sci U S A 2003;100(Suppl. 1):11881-11888.
19. Boyer LA, Plath K, Zeitlinger J, Brambrink T, Medeiros LA, Lee TI, et al. Polycomb complexes repress developmental regulators in murine embryonic stem cells. Nature 2006;441:349-353.
20. Lee TI, Jenner RG, Boyer LA, Guenther MG, Levine SS, Kumar RM, et al. Control of developmental regulators by Polycomb in human embryonic stem cells. Cell 2006;125:301-313.
21. Bernstein BE, Mikkelsen TS, Xie X, Kamal M, Huebert DJ, Cuff J, et al. A bivalent chromatin structure marks key developmental genes in embryonic stem cells. Cell 2006;125:315-326.
22. Kanai-Azuma M, Kanai Y, Gad JM, Tajima Y, Taya C, Kurohmaru M, et al. Depletion of definitive gut endoderm in Sox17-null mutant mice. Development 2002;129:2367-2379.
23. Cho CH, Parashurama N, Park EY, Suganuma K, Nahmias Y, Park J, et al. Homogeneous differentiation of hepatocyte-like cells from embryonic stem cells: applications for the treatment of liver failure. FASEB J 2008;22:898-909.
24. Gil J, Peters G. Regulation of the INK4b-ARF-INK4a tumour suppressor locus: all for one or one for all. Nat Rev Mol Cell Biol 2006;7:667-677.
25. Akasaka T, van Lohuizen M, van der Lugt N, Mizutani-Koseki Y, Kanno M, Taniguchi M, et al. Mice doubly deficient for the Polycomb Group genes Mel18 and Bmi1 reveal synergy and requirement for maintenance but not initiation of Hox gene expression. Development 2001;128:1587-1597.
26. Dovey JS, Zacharek SJ, Kim CF, Lees JA. Bmi1 is critical for lung tumorigenesis and bronchioalveolar stem cell expansion. Proc Natl Acad Sci U S A 2008;105:11857-11862.
27. Fasano CA, Dimos JT, Ivanova NB, Lowry N, Lemischka IR, Temple S. shRNA knockdown of Bmi-1 reveals a critical role for p21-Rb pathway in NSC self-renewal during development. Cell Stem Cell 2007;1:87-99.
28. Bruggeman SW, Hulsman D, Tanger E, Buckle T, Blom M, Zevenhoven J, et al. Bmi1 controls tumor development in an Ink4a/Arf-independent manner in a mouse model for glioma. Cancer Cell 2007;12:328-341.
29. Serrano M, Lee H, Chin L, Cordon-Cardo C, Beach D, DePinho RA. Role of the *INK4a* locus in tumor suppression and cell mortality. Cell 1996;85:27-37.
30. Lu SC, Alvarez L, Huang ZZ, Chen L, An W, Corrales FJ, et al. Methionine adenosyltransferase 1A knockout mice are predisposed to liver injury and exhibit increased expression of genes involved in proliferation. Proc Natl Acad Sci U S A 2001;98:5560-5565.
31. Sakamoto H, Oyamada M, Enomoto K, Mori M. Differential changes in expression of gap junction proteins connexin 26 and 32 during hepatocarcinogenesis in rats. Jpn J Cancer Res 1992;83:1210-1215.
32. Reya T, Clevers H. Wnt singnaling in stem cells and cancer. Nature 2005;434:843-850.
33. Wiederschain D, Chen L, Johnson B, Bettano K, Jackson D, Taraszka J, et al. Contribution of polycomb homologues Bmi-1 and Mel-18 to medulloblastoma pathogenesis. Mol Cell Biol 2007;27:4968-4979.
34. Douglas D, Hsu JH, Hung L, Cooper A, Abdueva D, van Doorninck J, et al. BMI-1 promotes ewing sarcoma tumorigenicity independent of CDKN2A repression. Cancer Res 2008;68:6507-6515.
35. Orland V. Polycomb, epigenomes, and control of cell identity. Cell 2003;112:599-606.
36. Zhang W, Glöckner SC, Guo M, Machida EO, Wang DH, Easwaran H, et al. Epigenetic inactivation of the canonical Wnt antagonist SRY-box containing gene 17 in colorectal cancer. Cancer Res 2008;68:2764-2772.

Radiotherapy and Oncology 96 (2010) 231–235

Contents lists available at ScienceDirect

Radiotherapy and Oncology

journal homepage: www.thegreenjournal.com

Particle beam radiotherapy

Comparison of efficacy and toxicity of short-course carbon ion radiotherapy for hepatocellular carcinoma depending on their proximity to the porta hepatis

Hiroshi Imada [a,b,*], Hirotoshi Kato [a], Shigeo Yasuda [a], Shigeru Yamada [a], Takeshi Yanagi [a], Riwa Kishimoto [a], Susumu Kandatsu [a], Jun-etsu Mizoe [a], Tadashi Kamada [a], Osamu Yokosuka [b], Hirohiko Tsujii [a]

[a] National Institute of Radiological Sciences, Chiba, Japan; [b] Department of Medicine and Clinical Oncology, Chiba University, Japan

ARTICLE INFO

Article history:
Received 27 April 2009
Received in revised form 4 March 2010
Accepted 21 May 2010
Available online 25 June 2010

Keywords:
Radiotherapy
Carbon ion
Hepatocellular carcinoma
Porta hepatis

ABSTRACT

Background and purpose: To compare the efficacy and toxicity of short-course carbon ion radiotherapy (C-ion RT) for patients with hepatocellular carcinoma (HCC) in terms of tumor location: adjacent to the porta hepatis or not.

Materials and methods: The study consisted of 64 patients undergoing C-ion RT of 52.8 GyE in four fractions between April 2000 and March 2003. Of these patients, 18 had HCC located within 2 cm of the main portal vein (porta hepatis group) and 46 patients had HCC far from the porta hepatis (non-porta hepatis group). We compared local control, survival, and adverse events between the two groups.

Results: The 5-year overall survival and local control rates were 22.2% and 87.8% in the porta hepatis group and 34.8% and 95.7% in the non-porta hepatis group, respectively. There were no significant differences ($P = 0.252$, $P = 0.306$, respectively). Further, there were no significant differences in toxicities. Biliary stricture associated with C-ion RT did not occur.

Conclusions: Excellent local control was obtained independent of tumor location. The short-course C-ion RT of 52.8 GyE in four fractions appears to be an effective and safe treatment modality in the porta hepatis group just as in the non-porta hepatis group.

Hepatocellular carcinoma (HCC) is one of the most common malignant tumors worldwide and is the third leading cause of death from cancer [1]. Various therapeutic options are presently available for patients with HCC. In radiotherapy, the role for patients with HCC was previously limited and unsatisfactory on the basis of its poor hepatic tolerance to irradiation [2,3]. Technological advances have made it possible to deliver a higher dose of radiation to focal liver tumors accurately, reducing the degree of toxicity [4–7]. Proton beam therapy was shown to be effective and safe for HCC, mainly due to its excellent dose distribution at the end of the beam path, called the Bragg peak [8–10]. Carbon ion beams also possess the Bragg peak, and they provide excellent dose distribution to the target volume by specified beam modulations [11–15]. They have advantageous biological and physical properties that result in a higher cytocidal effect than that of photons and protons [16–19]. Since 1995, carbon ion radiotherapy (C-ion RT) has been performed for treatment of HCC, and clinical trials were initiated at the National Institute of Radiological Sciences (NIRS).

In terms of HCC adjacent to the porta hepatis, treatment with minimal invasiveness and complications is an important issue. Surgical resection is the standard of curative treatment, but it is restricted to selected patients due to degradation of hepatic function [20,21]. Liver transplantation is a curative treatment of HCC, but it is often not feasible [22–24] and a shortage of donors also limits its possibilities. Radiofrequency ablation (RFA) and other ablative techniques obtain excellent local control, but are limited largely to small HCCs [25–27]. In the presence of blood vessels contiguous with tumor, blood flow reduces the thermal effects of RFA [28–30]. In addition, biliary complications after RFA for HCC adjacent to the porta hepatis sometimes occur, resulting in septic complications and liver failure [31].

We have already reported that C-ion RT used for the treatment of HCC is safe and effective [17,19]. In this study, patients were stratified into two groups according to tumor localization: adjacent to the porta hepatis or not. We compared the treatment effect and toxicity between the two groups retrospectively.

Materials and methods

Patients

Between April 2000 and March 2003, 64 patients with HCC underwent 52.8 GyE/4-fraction C-ion RT in a phase I/II clinical trial or phase II clinical trial at NIRS. The phase I/II clinical trial was carried out from April 2000 to March 2001, and the phase II clinical

* Corresponding author. Address: Research Center for Charged Particle Therapy, National Institute of Radiological Sciences, 4-9-1, Anagawa, Inage-ku, Chiba 263-8555, Japan.
E-mail address: h_imada@nirs.go.jp (H. Imada).

0167-8140/$ - see front matter © 2010 Elsevier Ireland Ltd. All rights reserved.
doi:10.1016/j.radonc.2010.05.019

Table 1
Patient and tumor characteristics.

	Total	Porta hepatis group	Non-porta hepatis group	*P*
N	64	18	46	
Gender, *n* (%)				>0.999
Male	48 (75)	14 (78)	34 (74)	
Female	16 (25)	4 (22)	12 (26)	
Age (years)				0.736
Median	69	68	69	
Range	37–84	51–79	37–84	
Child-Pugh classification, *n* (%)				0.198
A	49 (77)	16 (89)	33 (72)	
B	15 (23)	2 (11)	13 (28)	
Stage (UICC 5th), *n* (%)				0.438
II	23 (36)	5 (28)	18 (39)	
IIIA	32 (50)	9 (50)	23 (50)	
IVA	9 (14)	4 (22)	5 (11)	
Maximum tumor diameter (mm)				0.725
Median	40.0	36.5	40.0	
Range	12–120	21–120	12–112	
Vascular invasion				0.066
Yes	45 (70)	16 (89)	29 (63)	
No	19 (30)	2 (11)	17 (37)	
Number of tumors, *n* (%)				0.676
Single	56 (88)	15 (83)	41 (89)	
Multiple	8 (12)	3 (17)	5 (11)	

Abbreviations: UICC = International Union against cancer.

trial was sequentially performed from April 2001 to March 2003. The eligibility criteria were previously reported [17]. HCC was diagnosed by needle biopsy in all patients. Prior to treatment, all patients gave their informed consent in writing in accordance with the Declaration of Helsinki. These clinical trials were approved by the ethics committees at NIRS. Eighteen of the 64 patients had HCC located within 2 cm from the main portal vein, and the other 46 had HCC far from the porta hepatis.

Background data of the patients and tumors are presented in Table 1. The enrolled patients consisted of 48 males and 16 females. Median age was 69 years (range, 37–84). Child-Pugh classification of the degree of liver impairment was as follows: 49 patients were categorized as Class A (scores, 5–6), and 15 patients as Class B (scores, 7–9). Twenty-three patients had Stage II, 32 had Stage IIIA, and 9 had Stage IVA. By the Barcelona Clinic Liver Cancer staging classification [32,33], 2 patients had Stage A and 16 had Stage C in the porta hepatis group, and 15 had Stage A, 2 had Stage B, and 29 had Stage C in the non-porta hepatis group. Median maximum tumor diameter was 40 mm (range, 12–120). Forty-five patients had vascular invasion. Fifty-six patients had a solitary mass and 8 had multiple tumors.

Pretreatment evaluation

Laboratory values collected for all patients included complete blood cell counts, liver and renal function tests, electrolytes, HBV and HCV titers, and α-fetoprotein (AFP). Abdominal triphasic CT or MRI was performed for evaluation of the extent of HCC.

C-ion RT

The carbon ion beam used for radiotherapy was generated by the heavy ion medical accelerator in Chiba developed by NIRS in 1993. The accelerator system and the biophysical characteristics of the carbon ion beam have been previously described [13–15]. For modulation of the Bragg peak of the beam to conform to the target volume, the beam lines in the treatment room are equipped with a pair of wobbler magnets, beam scatterers, ridge filters, multileaf collimators, and a compensation bolus.

Before therapeutic planning, all patients had metallic markers (iridium seeds, 0.5 mm in diameter and 3 mm in length) implanted near the tumor to obtain precise treatment positioning. The irradiation fields were established with a three-dimensional therapy plan on the basis of 5-mm-thick CT images. The planning target volume was defined according to the shape of the tumor plus a 1.0–1.2 cm margin. To reproduce the target position accurately, a low-temperature thermoplastic sheet (Shellfitter, Kuraray, Osaka, Japan), a customized cradle (Moldcare, Alcare, Tokyo, Japan), and a respiratory gated irradiation system [34] were used in the CT planning and radiotherapy performance. The radiation field was confirmed and corrected by orthogonal fluoroscopy and radiography immediately before each treatment session.

Irradiation doses were expressed in Gray equivalents (GyE = carbon physical dose [in Gray] × relative biologic effectiveness). The relative biologic effectiveness value of carbon ions was assumed to be 3 at the distal part of the spread-out Bragg peak [35]. C-ion RT was given once daily, 4 days a week, for four fractions in 1 week. The dose per fraction was 13.2 GyE, so all patients received a total dose of 52.8 GyE.

Follow-up and evaluation criteria

All patients were assessed according to a predetermined schedule. After C-ion RT, patients were evaluated on the basis of physical examinations and blood tests once a month for the first year, once every 3 months for the following year, and once every 3–6 months thereafter. Contrast-enhanced CT or MRI was performed every 3 months for the first 2 years and every 6 months thereafter. Local control was defined as no sign of regrowth or new tumor in the treatment volume. Local recurrence was defined as failure of local control. Overall survival was measured from the starting date of treatment until the date of death from any cause. Cause-specific survival was defined as the interval between the starting date of treatment and the date of death from liver failure or HCC. Disease-free survival was defined as the interval between the starting date of treatment and the date of the diagnosis of the first recurrence or death from any cause. Acute and late toxicities were assessed using the National Cancer Institute Common Criteria, version 2.0, and the Radiation Therapy Oncology Group/European Organization for Research and Treatment of Cancer late radiation morbidity scoring scheme. Liver toxicity in late phase was assessed by Child-Pugh score, a commonly used marker of hepatic functional reserve in chronic liver disease.

Statistical analysis

Statistical analyses were performed using SPSS version 12.0 (SPSS Inc., Chicago, IL). For continuous variables, non-parametric tests (Mann–Whitney *U* test) were used. For categorical data, chi-squared test or Fisher's exact test was used. The Kaplan–Meier method was used for calculation of local control and survival rates, and the survival curves were compared by log-rank test. Statistical significance was considered if $P < 0.05$ (*P*-values from two-sided tests).

Results

There were no significant differences in sex, age, Child-Pugh classification, clinical stage, maximum tumor diameter, and tumor number between the two groups. The porta hepatis group exhibited greater vascular invasion than the non-porta hepatis group ($P = 0.066$).

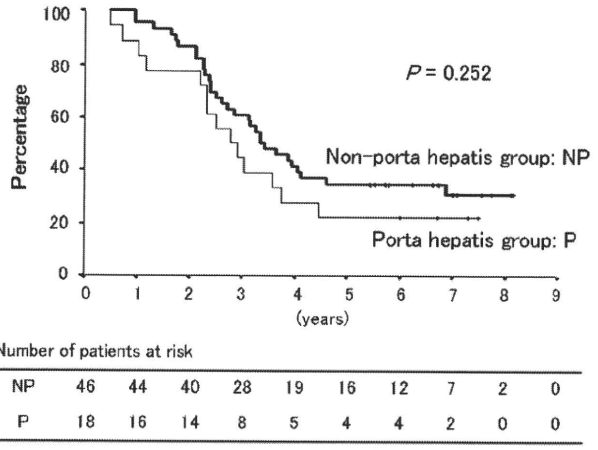

Number of patients at risk

NP	46	44	40	28	19	16	12	7	2	0
P	18	16	14	8	5	4	4	2	0	0

Fig. 1. Overall survival rate according to tumor localization. Overall survival rates after 3 and 5 years were 44.4% and 22.2% in the porta hepatis group and 60.9% and 34.8% in the non-porta hepatis group, respectively. There were no significant differences between the two groups ($P = 0.252$).

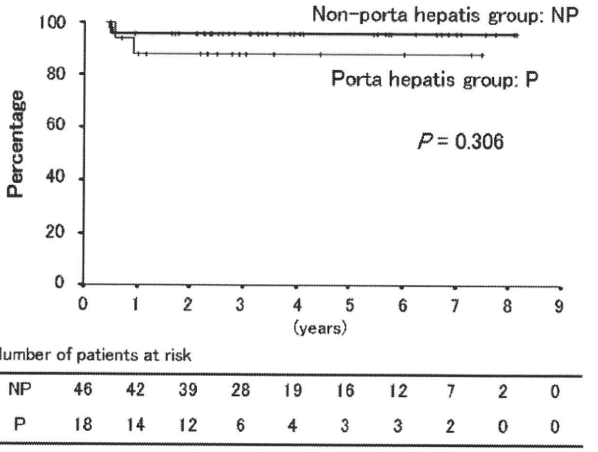

Number of patients at risk

NP	46	42	39	28	19	16	12	7	2	0
P	18	14	12	6	4	3	3	2	0	0

Fig. 2. Local control rate according to tumor localization. Local control rates after both 3 and 5 years were 87.8% in the porta hepatis group and 95.7% in the non-porta hepatis group. There were no significant differences between the two groups ($P = 0.306$).

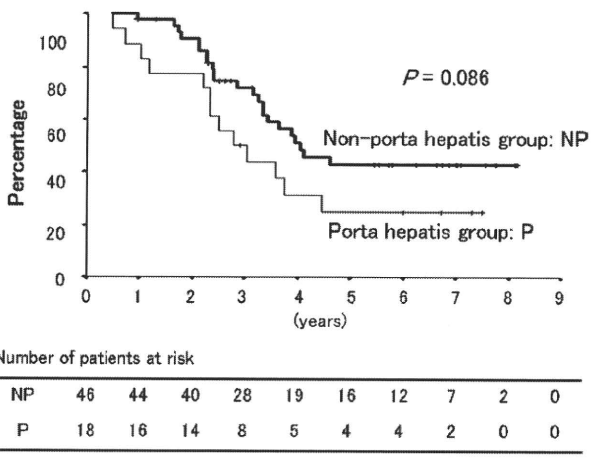

Number of patients at risk

NP	46	44	40	28	19	16	12	7	2	0
P	18	16	14	8	5	4	4	2	0	0

Fig. 3. Cause-specific survival rate according to tumor localization. Cause-specific survival rates after 3 and 5 years were 50.0% and 25.0% in the porta hepatis group and 72.3% and 42.8% in the non-porta hepatis group, respectively. The porta hepatis group showed a trend towards inferior outcome compared to the non-porta hepatis group ($P = 0.086$).

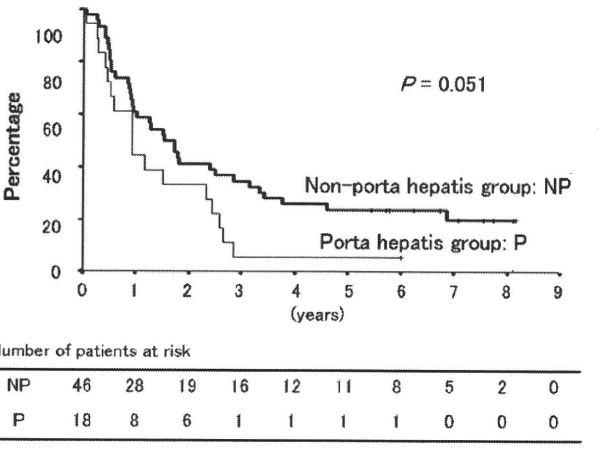

Number of patients at risk

NP	46	28	19	16	12	11	8	5	2	0
P	18	8	6	1	1	1	1	0	0	0

Fig. 4. Disease-free survival rate according to tumor localization. Disease-free survival rates after both 3 and 5 years were 5.6% in the porta hepatis group, and they were 34.8% and 23.9% in the non-porta hepatis group, respectively. The porta hepatis group showed a trend towards inferior outcome compared to the non-porta hepatis group ($P = 0.051$).

The median observation period for survival was 34 months (range, 6–90 months) in the porta hepatis group and 41 months (range, 11–98 months) in the non-porta hepatis group. Four patients were alive at last follow-up and 14 had died in the porta hepatis group, and 15 were alive at last follow-up and 31 had died in the non-porta hepatis group. Overall survival rates after 3 and 5 years were 44.4% [95% confidence interval (CI), 22–67] and 22.2% [95% CI, 3–41] in the porta hepatis group and 60.9% [95% CI, 47–75] and 34.8% [95% CI, 21–49] in the non-porta hepatis group, respectively (Fig. 1). Local control rates after both 3 and 5 years were 87.8% [95% CI, 72–104] in the porta hepatis group and 95.7% [95% CI, 90–102] in the non-porta hepatis group, respectively (Fig. 2). There were no significant differences between the two groups in overall survival and local control rates ($P = 0.252$, $P = 0.306$, respectively). Cause-specific survival rates after 3 and 5 years were 50.0% [95% CI, 27–73] and 25.0% [95% CI, 4–46] in the porta hepatis group and 72.3% [95% CI, 59–86] and 42.8% [95% CI, 27–58] in the non-porta hepatis group, respectively (Fig. 3). Disease-free survival rates after both 3 and 5 years were 5.6% [95% CI, −5 to 16] in the porta hepatis group, and they were 34.8% [95% CI, 21–49] and 23.9% [95% CI, 12–36] in the non-porta hepatis group, respectively (Fig. 4). In the cause-specific and disease-free survival rates, the porta hepatis group showed a trend towards inferior outcome compared to the non-porta hepatis group ($P = 0.086$, $P = 0.051$, respectively).

Toxicities in early phase are shown in Table 2. Adverse events of grade 3 or more were compared between the two groups. There were no significant differences in hepatic and hematologic toxicities ($P > 0.999$, $P = 0.190$, respectively). As to Child-Pugh score in late phase, cases with changes in Child-Pugh score within 1-point increase were 13 in the porta hepatis group and 41 in the non-porta hepatis group. Those with changes in score increasing by at least 2 points were five in each of the groups. There were no significant differences between the two groups in terms of change in Child-Pugh score (≤ 1 vs. ≥ 2) ($P = 0.128$) (Table 3). In terms of other non-hematologic toxicities such as skin and gastrointestinal toxicities, toxicities of grade 3 or higher did not occur. No patient had biliary stenosis associated with C-ion RT.